IN VIVO QUANTIFICATION OF ALUMINUM

APPLICATION OF SPECTRAL DECOMPOSITION ANALYSIS TO *IN VIVO* QUANTIFICATION OF ALUMINUM

By

DARIA C. COMSA, M.Sc.

A Thesis
Submitted to the School of Graduate Studies
in Partial Fulfillment of the Requirements
for the Degree
Master of Science

McMaster University

MASTER OF SCIENCE (2003) McMaster University

(Medical Physics) Hamilton, Ontario

TITLE: **Application of Spectral Decomposition Analysis to *In Vivo* Quantification of Aluminum**

AUTHOR: Daria C. Comsa, M.Sc. (Babes-Bolyai University, Romania)

SUPERVISOR: Professor William V. Prestwich

NUMBER OF PAGES: vii, 60.

Abstract

Aluminum is a non-essential trace element that accumulates in human bone tissue (Nayak, 2002). Its toxic effects are cumulative and result in painful forms of renal osteodystrophy, most notably adynamic bone disease and osteomalacia, but also other forms of disease (Yokel, 2001; Cannata-Andia, 2002).

Presently, histological tests of bone biopsies are the only approach for the diagnosis of aluminum-related pathologies (Malluche, 2002). Neutron Activation Analysis was proposed as an alternative method for quantifying aluminum. The Trace Element Group at McMaster University has developed an *in vivo* procedure for detecting aluminum levels in the bones of the hand, exploiting an accelerator-based approach. A minimum detectable limit (MDL) of 1.14mg of aluminum could be distinguished for a local dose to the hand of 48mSv (Pejovic-Milic, 2001). For the procedure to be clinically effective, the MDL should be comparable to the levels normally contained in healthy subjects (0.3-0.4 mg Al). Further refining of the method is therefore necessary.

This dissertation presents an improved algorithm for data analysis, based on Spectral Decomposition. Following phantom measurements, a new MDL of (0.7±0.1)mg Al was reached for a local dose of (20±1)mSv, representing an improvement by a factor of 1.60±0.04. In addition, a time-dependent variant of this algorithm was proposed.

The study also addresses the feasibility of a new data acquisition technique, the electronic rejection of the coincident events detected by the NaI(Tl) system. It is expected that the application of this technique, together with Spectral Decomposition Analysis, would provide an acceptable MDL for the method to be valuable in a clinical setting.

Acknowledgments

My words cannot express my thanks to my supervisor, Dr. William Prestwich. I appreciate his advice and encouragement, and above this, he is a role model in my life and work. I know I'll try hard not to disappoint him.

From the beginning, Dr. McNeill was involved in my quest for the right project, and continued to support my work throughout. It was Fiona's confident smile that made me choose McMaster and for this I am grateful.

Thank you to Dr. Colin Webber for so kindly revising my work and dedicating time to my thesis. Thank you to Dr. David Chettle for his encouraging interest in my work and helpful remarks.

I value the help and friendship of everybody in the accelerator lab. They must have realized how much I missed my family, since they had become one. Thank you to Scott McMaster, who always found time to listen to my problems in the lab and "resources" to solve them. Thank you Jason for hours spent working with me on the accelerator and also for appreciating my baking skills. For quite a few generations of phantoms and other equipment my appreciation goes to John Cave. Thanks to Kenrick Chin, on whose expertise in electronics and programming a great part of my work relied.

In these two years, wonderful friends made the problems easier to surpass and taught me that the joy is worth sharing. Thank you Marija for the color you brought to my life, you *are* a true artist. Anne Marie, you'll always be our little white one! Thank you to Aslam, SooHyun and Ryan for their valuable advice and help.

There was one person who was understanding and accepting of the time I spent on this work. It is time now to return all the love and support to my dear husband, Rares.

I wish my parents were closer these days so I could thank them more often for the years and trust they invested in me. This work is dedicated to them.

Table of contents

LIST OF FIGURES AND TABLES

Chapter 1. Introduction

Aluminum routes of exposure and associated toxicity

Aluminum (Al) is a nonessential metal that occurs normally in the body tissues of humans as a toxic trace element. Its impact on biological systems has been the subject of a wealth of studies during the past few decades. A series of medical conditions associated with Al toxicity have motivated investigations on its routes of exposure, bioavailability, and toxicokinetics. The general population is mainly exposed to Al via ingestion, inhalation, and iatrogenic administration. Occupational exposure was also observed; elevated levels of Al were reported among workers from the Al processing and welding industry, primarily affecting their respiratory system (Riihimäki *et al.*, 2000; Hjortsberg *et al.*, 1999).

Natural Al constitutes about 8% of the earth surface. Acid rain can release Al from the soil, increasing free Al in the environment and the surface waters. When the soil pH is lower than 4.5-5.0, Al is solubilized in the soil water and absorbed by plant roots (Matsumoto, 2000). Therefore, many types of food grown in soil contain Al. Apart from this, food additives also contain a substantial amount of Al. Leaching of Al from beverage cans and cookware was investigated as well (Lin et al, 1997). It was estimated that about 20% of daily intake of Al comes from cooking utensils (pans, pots, kettles, and trays) made of Al (Greger *et al.*, 1985, Lin *et al.*, 1997). An average human consumes daily 3-100mg Al through food and drinks (Lione, 1983; Yokel *et al.*, 2001). Recent extensive studies showed that an amount of 3.4mg Al is present in the average daily diet in the United Kingdom (Ysart *et al.*, 2000). The mean Al intake reported in a total diet study was 10mg/day for an adult male, and 7mg/day for an adult female (Flarend *et al.*, 2001). The primary Al sources for man were synthesized in a review paper by Yokel (Yokel *et al.*, 2001). Based on Al bioavailability data, he shows that the primary normal source of Al for man is food (0.08-0.5μg/kg/day), while water provides only about 1% of normal daily human Al intake 0.005μg/kg/day. Although the intestinal absorption of Al is

as low as 0.1% (Flaten *et al.*, 2001), many organic dietary compounds are potential chelators of Al and may enhance its absorption (Deng *et al.*, 2000; Venturini-Soriano *et al.*, 2001). In addition, it was observed that certain pathological conditions could also increase the intestinal absorption of Al.

Following oral exposure, the retention of Al was reported in brain, bone, kidneys, muscle and heart (Yokel *et al.*, 1985, Anthony *et al.*, 1986, Chan *et al.*, 1988). Several neuropathologies have been attributed to Al intoxication. They include memory loss, tremor, jerking movements, impaired coordination, loss of curiosity, ataxia, generalized convulsions, etc. Behavioral toxicity of Al, manifested through agitation, confusion, seizures, coma, and sudden death, was also reported (Bakir *et al.*, 1986). The impact of Al on the musculoskeletal system was observed in more chronic poisoning. Osteomalacia or aplastic bone disease (associated with painful spontaneous fractures, hypercalcemia, tumorous calcinosis), proximal myopathy, and failure to respond to vitamin D_3 therapy are common features of Al-induced musculoskeletal toxicity (Alfrey, 1984). Both clinical and experimental exposures to high doses of Al were found to inhibit remodeling, to slow osteoblast and osteoclast activities and to produce osteomalacia and adynamic bone disease (Jefferey *et al.*, 1996). It has been suggested that the observed cardiac hypertrophy in hemodialysis patients may be caused in part by Al.

Intake of Al via the respiratory system from unpolluted air is generally quite low, below 4μg per day. In industrial areas, where Al levels in air may be much higher, intakes can exceed 100μg per day (Yokel *et al.*, 2001). Occupationally exposed workers may inhale up to 0.6mg per day (Yokel *et al.*, 2001). Following inhalation exposure, the effects of Al are mainly exerted on the respiratory system. Workers in the Al industry develop asthma, cough, lung fibrosis, or decreased pulmonary function, but whether these effects are due only to Al is questionable (California EPA, 2001).

Common iatrogenic sources of Al exposure are vaccines (150-850μg/dose) (Yokel *et al.*, 2001), Al hydroxide, used as an antacid and a phosphate binder, and some parenteral nutrition solutions. It is important to notice that parenteral administration of Al contaminated solutions results in 100% absorption (Yokel *et al.*, 2001). This results

in a greatly increased daily intake of Al for individuals consuming maximum recommended doses of Al-based over-the-counter drugs such as antacids and buffered acetylsalicylic acid. The World Health Organization has estimated that individuals who regularly ingest these Al-containing pharmaceuticals may ingest up to 5g per day. Moreover, chronic renal failure leads to decreased Al excretion and consequently enhances Al toxicity. Systemic Al intoxication was initially identified in patients with chronic renal failure, due to contamination of the haemodialysis fluids and intravenous solutions (Alfrey *et al.*, 1976). Currently Al toxicity has virtually disappeared in the dialysis population; however, sporadic toxic effects are still reported (Fernandez-Martin *et al.*, 2000; Berand *et al.*, 2001). Nevertheless, Al loading has been observed in patients with normal renal function who received long-term parenteral nutrition with Al-contaminated fluids (Bishop *et al.*, 1997; Ott *et al.*, 1983).

Aluminum distribution among tissues

Aluminum distributes unequally to all tissues throughout normal and Al-intoxicated humans (Alfrey, 1980; Di Paolo *et al.*, 1997). An initial distribution might be consistent with blood volume (Wilhelm *et al.*, 1990). Of the 30-50mg normal Al body burden, the skeletal system and lungs accumulate about 50% and 20%, respectively (ATSDR 1999). The brain has lower Al concentration than many other tissues. However, studies of Alzheimer's disease victims showed elevated brain Al contributing to the controversy concerning a possible role of Al in the etiology of this disease (Rondeau, 2002; Jansson, 2001). Al is also found in human skin, lower gastrointestinal tract, lymph nodes, adrenals, and parathyroid glands. The kinetics of Al in liver, bone, and kidney were generally dose independent (Nayak, 2002).

Analytical methods for aluminum quantification

Aluminum levels have been mostly quantified in blood and urine, as some of the most easily obtainable biological samples. A variety of analytical methods has been used in this purpose, including AMS (accelerator mass spectroscopy), graphite furnace atomic absorption spectrometry (GFAAS), flame atomic absorption spectrometry (FAAS), neutron activation analysis (NAA), inductively coupled plasma-atomic emission spectrometry (ICP-AES), inductively coupled plasma-mass spectrometry (ICPMS), and laser ablation microprobe mass analysis (LAMMA) (Maitani *et al.* 1994; Owen *et al.* 1994; Van Landeghem *et al.* 1994).

Although the sensitivity of these techniques allows measurement of what are considered normal levels of Al, the ubiquitous nature of this trace element makes the quantification a more challenging task due to contamination (Makjanic *et al.* 1998). Most importantly, it is believed that data collected using these techniques cannot be used to accurately correlate Al levels in biological materials to exposure and effect levels. For example, wide variations in blood and urine Al levels can occur because of differences in diet, intake of medication, state of health, the type of Al involved and the route of exposure (IDSP Report, 1992). In dialysis patients, Al blood levels did not correspond to the total body burden (Wilhelm, 1989). Animal research leads to the same conclusion. After five months of low-level exposure to Al oxide dust, rabbits' brains accumulated two and a half times the Al levels found in the non-exposed and lung levels were 158 times higher, but blood levels were only slightly raised (Röllin, 1991). Although a correlation may be found between high Al levels and Al induced bone disease, plasma Al levels do not predict well the presence of pathology (Jarava *et al.*, 2001; Kausz *et al.*, 1999). In a study of 258 patients, the sensitivity and specificity of Al plasma test were of only 65.2% and 76.7%, respectively (Kausz *et al.*, 1999).

Alternatively, the diagnosis of Al toxicity can be made by the desferrioxamine test. Intravenous desferrioxamine mobilizes Al accumulated in bone and other organs elevating blood Al levels. However, elevated Al levels may be found without the confirmed presence of a bone disease (Sebes, 2003). Moreover, serious side effects were

reported following chelation therapy, such as fatal blood infections, damage to hearing and vision, nausea, diarrhea, lowered blood pressure, etc. (D'Haase *et al.*, 1995; Pengloan *et al.*, 1987).

The only specific test to prove bone pathology remains the histochemical analysis of a bone biopsy. It was proved that bone is the most reliable tissue for assessing total body burden (Connor *et al.*, 1986; Faugere *et* Malluche, 1986). Iliac crest biopsies are stained with Al stain (*e.g.* aurine tricarboxilic acid which marks Al bright red). Accumulation of Al on the trabecular bone surface at the mineralization front is diagnostic of Al bone disease (Ellis *et al.*, 1982; Maloney *et al.*, 1982). In any event, bone biopsy is considered far too invasive to be proposed for medical monitoring.

The conclusion of the Industrial Disease Standards Panel in the 1992 Report to the Ontario Ministry of Labor was that "no acceptable tool capable of reliably determining whether, how much or where Al may be accumulating in the body is currently available". The Report also underlines the potential of Neutron Activation Analysis as a method for quantifying Al *in vivo*.

Literature review

The need for a non-invasive procedure for quantifying skeletal Al burden has encouraged researchers to explore Neutron Activation Analysis (NAA) as an *In Vivo* detection method. For the past three decades, this technique has been considered a criterion method to measure total body N, Ca, Cl, Na, P, and C in human subjects (Cohn, 1980).

The detection of Al imposes a few constraints on NAA. As detailed further in the Methodology chapter, when activating the stable isotope ^{27}Al, unwanted interferences can occur from activation of other isotopes present in human body. As various studies showed, a careful selection of the neutron source may overcome these interferences, resulting in superior detection sensitivity. As the dose delivered to the patient during NAA is also a limiting factor in the method's sensitivity, the available neutron fluence

rate and the efficiency of the gamma detection system play an important role in the success of this technique. Different neutron sources and detection systems were hence investigated for total or partial body NAA of Al. The most relevant results are summarized in Table I.

Table I. Review of significant studies on Al detection by *In Vivo* NAA.

Publication	Neutron source	Local Dose (mSv)	MDL (mg)
Ellis *et al.* (1987, Brookhaven)	Reactor thermal beam	20	0.4
Morgan *et al.* (1990 Swansea)	Moderated ^{252}Cf	20	3.4
Wyatt *et al.* (1993, Swansea)		36	2.2
Green and Chettle (1992, Birmingham)	Accelerator $^{3}H(^{1}H,n)^{3}He$	50	1.2
Pejovic-Milic (2001, McMaster)	Accelerator $^{7}Li(^{1}H, n)^{8}Be$	48	1.1

A thermal/epithermal neutron beam of the Brookhaven Medical Research Reactor was the neutron source of choice in a study by Ellis *et al.* (1987). Partial body (hand) Al NAA was performed on patients with end-stage renal failure. The high thermal neutron fluence rate available ($1.3x10^{7}n/cm^{2}/s$) resulted in a good degree of discrimination against the interference with phosphorus. Moreover, the minimum detectable limit (MDL), sufficiently low to detect normal levels of Al, was achieved for a reasonably low local dose.

However, research reactors are not widely available within the medical community and consequently the application of this technique is therefore limited. This encouraged the research group at Swansea, UK, to investigate an alternative neutron source, the radionuclide ^{252}Cf. A filtered ^{252}Cf source allowed Wyatt *et al.* (1993) to obtain a thermal neutron fluence rate of $3.2x10^{5}n/cm^{2}/s$. Although the low fluence rate was partially compensated for using a cyclic activation technique, the Brookhaven performance could not be reproduced.

An accelerator-based system for Al detection was then considered. This neutron source brings the advantage that the maximum neutron energy can be kept below the threshold for interfering neutron reactions. Also, the possibility of using a mobile accelerator opens the prospect of applying the method at a larger scale, enabling clinical studies at different sites of interest, *e.g.* mines, hospitals, Al contaminated areas, etc. A feasibility study was conducted at Birmingham, where the 3MV Dynamitron was used to generate neutrons via the reaction $^{3}H(^{1}H,n)^{3}He$. During this study, attempts to optimize the irradiation parameters, accompanied by microdosimetry measurements, pointed out the relevance of the later for the procedure. The maximal detection sensitivity with respect to effective dose was reached for considerably lower proton energy than the maximum sensitivity relating to absorbed dose. Another important point of the same study regards the microdosimetry technique itself. For neutron energies below 500keV the recoil particle range becomes very short resulting in incorrect sampling of the spectrum inside the gas cavity. The study also evaluated the possibility of using high-resolution Ge detectors instead of NaI(Tl) detectors. Their results (Table I) encouraged the authors to predict a number of further improvements to an accelerator-based system that would be expected to significantly increase the sensitivity of the method. Increased NaI detectors size, an optimal irradiation cavity based on neutron transport calculations, more precise calculation of optimum source energy, better dose delivery, and a more sophisticated spectroscopic data reduction were some of the anticipated developments.

At McMaster University, a feasibility study for Al detection was initiated in 1993 (Palerme, 1993). This work investigated the neutron sources available within the facilities, the reactor and the accelerator, as potential sources for a system of *in vivo* detection of Al. As expected, the interference reactions arising from the interaction of fast neutrons with phosphorus and silicon in the hand were seen to considerably reduce the effectiveness of the reactor as a neutron source. The accelerator-based neutron source was reported as a feasible alternative.

Following this preliminary pilot study, the Trace Element Group researchers at McMaster have begun a comprehensive investigation of the KN-accelerator (Pejovic-

Milic, 1998; 2001). The previous performance of an accelerator-based NAA study was repeated at McMaster (Table I). With the purpose of further decreasing the dose to the patient, an irradiation cavity designed based on Monte Carlo simulations is currently under development. However, improvement of the system is required for achieving a MDL as low as the normal Al levels in patients before clinical studies can be initiated.

The motivation of the present work resides therefore in the necessity of attaining a higher sensitivity in detecting Al by *in vivo* NAA.

Chapter 2. Methodology

2.1. Study design

Justification for the methodology

Neutron activation analysis (NAA) is now an established method of detection of trace elements. This technique has been available since the late sixties and it is of special value in a variety of clinical applications involving bone composition measurements. The possibility of performing non-invasive analysis, high specificity based on the individual characteristics of the induced radionuclides, relative freedom from matrix and interference effects, and the capability for multi-element determination are some of the advantages of NAA over other methods used in the investigation of elemental composition in humans.

The principles on which activation analysis is founded are simply the irradiation of the sample with neutrons, a process which leads to activation of the nuclide of interest into a radioactive isotope, followed by the detection of the characteristic gamma rays emitted by the latter. The number of events detected provides a measure of the quantity of original nuclide. Using the concepts of nuclear transformation, decay, and radiation detection, an equation which describes the count rate expected from a neutron activated element in a sample can be derived. The number of counts recorded during a count time t_c, following an irradiation time t_i, and transfer time t_t, is:

$$C = \frac{h \cdot m \cdot \% \cdot N_A \cdot \phi \cdot f \cdot \sigma_0}{A \cdot \lambda}\left[1 - e^{-\lambda t_i}\right]\left[e^{-\lambda t_t}\right]\left[1 - e^{-\lambda t_c}\right]$$

where: h - the absolute efficiency of the detector set-up, including effects of geometry, detector response, and self-shielding, m - mass of the irradiated element (g), % - abundance of the isotope of interest, N_A - Avogadro's number (atoms/g atom), A - atomic mass of the irradiated element (AMU), ϕ - thermal neutron fluence rate (neutrons/cm^2/s),

f - gamma-ray emission probability per decay, σ_0 - absorption cross-section at 2200m/s and λ - decay constant of the radioisotope produced. The expression clearly indicates the activity of the irradiated material generated by the thermal neutron flux at the location of the irradiation, corrected for decay before and during counting.

The activation procedures vary widely with respect to neutron sources, moderators, site of activation, and detection systems. It is of crucial importance to examine the characteristics of each of these basic components in order to determine the method the most appropriate for the detection of a particular element. For Al detection, particular care is required when choosing the neutron source due to the occurrence of reactions that interfere with the nuclear reaction of interest. An accelerator has a number of advantages over other available neutron sources. By varying the energy of the protons onto the target, the maximum neutron energy can be controlled and set below the threshold of the interfering reactions. A sufficiently intense thermal fluence rate, which would result in a high activation, can be obtained by moderation of the neutron beam. Moreover, accelerators are more readily available and possibly more mobile than nuclear reactors.

The methodology for sample irradiation and detection employed in the current study is based on proposals from previous projects on Al detection conducted at McMaster University. Between 1993 and 2001 intensive work was dedicated to Al detection *in vivo* (Palerme, 1993; Pejovic-Milic, 1998, 2001). Given the reported optimal irradiation and detection parameters in these studies, the immediate purpose of the present project is the investigation of a means of lowering the detection sensitivity of the method, while keeping the total dose to the patient as low as possible. For the method to be useful in a clinical setting, its sensitivity should allow detection of levels below the levels found in healthy individuals. In the case of Al, for which NAA is performed on the patient's hand and wrist, the desired sensitivity range would typically be 0.3-0.4 mg Al (ICRP 23). The MDL value of 1.14 mg (Pejovic-Milic, 2001) obtained in a previous

study at McMaster is about three times higher than the amount of Al expected in a typical person. In these conditions, improvement with at least a factor of 3 in the MDL value would be necessary.

Study proposal

The present study was developed as a combination of a new experimental tactic and data analysis optimization. Experimentally, a detection setting was proposed and tested, namely counting of the irradiated sample using electronic rejection of coincidences. In a typical spectrum of a hand, Al signal is accompanied and partly overlapped by features from sodium and chlorine isotopes. Because both isotopes present so-called "cascade" decay, one can make use of the summation effect and reject coincidences from the original spectrum, leaving a cleaner and more specific spectrum of the element of interest, Al.

Examination of the counting statistics contribution to the uncertainty in the net peak area and in controlling detection limits showed the importance of maximizing peak-to-background ratio, counting rate and counting time (Ortec, AN59, 2001). The MDL is calculated based on the uncertainty in the number of counts specific for the element of interest when a zero-concentration sample is measured. Therefore, the higher the number of counts that the method is able to recover from a spectrum, the lower the statistical error involved and, by consequence, the MDL. The spectrum reflects the detector response to different energy gamma rays, its resolution, detection geometry, attenuation and scattering. A complex shape includes the following features: backscattering peak, pair escape peaks, Compton edge and continuum, photopeak, annihilation quanta from pair production. Traditionally, only the counts in the photopeak corresponding to the element of interest are considered in the data analysis (*e.g.* Levenberg-Marquardt method). An innovation of the method proposed in the present study, based on spectral

decomposition analysis, is the use of the complete detector response to the energies and characteristics of each element in the spectrum. For this purpose, a library of single-element spectra is to be built up, covering all major features of the combined spectrum, followed by the summation of the individual spectra with varying intensities, until the least squares difference between the experimental and fitted spectra is obtained. Recovery of a higher number of counts from the spectrum is expected to result in lower uncertainties and therefore in a lower MDL.

2.2. Instruments and Procedure

2.2.1. Neutron Activation Parameters and Procedure

Introduction

There are three neutron reactions with adequate cross-sections that could serve Al detection purposes. As summarized in Table II, each of these reactions can be accompanied and disturbed by direct interferences from neutron reactions with other elements present in the human body.

Table II. Neutron reactions with ^{27}Al and possible interferences.

Reaction	Interfering reaction
$^{27}Al(n,\alpha)^{24}Na$	$^{23}Na(n,\gamma)^{24}Na$
$^{27}Al(n,p)^{27}Mg$	$^{26}Mg(n,\gamma)^{27}Mg$
$^{27}Al(n,\gamma)^{28}Al$	**$^{31}P(n,\alpha)^{28}Al$**

For the first two cases, the interferences are thermal neutron reactions, and their occurrence is very probable due to the moderation of the neutrons within the body. By contrast, for the (n,γ) reaction, its (n,α) interference is a fast neutron reaction with the threshold at 1.95MeV. Choosing a source spectrum with maximum energy below this threshold will therefore eliminate the interference from Phosphorus. This (n,γ) reaction was the one considered in all previous trials for Al detection and was also investigated in the present study.

KN Accelerator as neutron source

A Van de Graaff type accelerator is part of the facility for neutron activation used at McMaster University Accelerator Laboratory. The accelerator is based on a simple principle: a high potential difference is built up and maintained on a conducting surface

by the continuous transfer of positive static charges from a moving belt to the surface. A hydrogen reservoir located inside the high-voltage terminal constitutes the ion source. Protons are accelerated from source to a target by the electric voltage between the high-voltage supply and ground.

Acceleration of protons onto a lithium target leads to production of neutrons as a result of the $^{7}Li(p,n)^{7}Be$ reaction, with a threshold of 1.88MeV. The target used is a thick lithium target and therefore a spectrum of neutron energies is produced, rather then discrete values. Complex neutron spectra result, which are functions of proton energy and angle from the beam axis.

For an optimal and reproducible activation experiment, the characterization of the neutron energy spectrum, along with the investigation of fluence rate is of critical importance. Knowledge and control of maximum neutron energy are required for avoiding threshold interference reactions. On the other hand, since only the thermal component of the neutron spectrum contributes to activation of ^{27}Al, maximization of the thermal neutron fluence rate is needed for acquiring maximum activation per total dose to the patient. For this purpose, both experimental (Pejovic-Milic, 1998, 2001; Arnold, 2000; Aslam, 2001) and analytical investigations (Arnold, 2000; Aslam, 2001, 2003a) of McMaster accelerator as a neutron source have been conducted in several projects.

Preliminary measurements performed using ^{115}In foils activation (Pejovic-Milic, 1998) revealed an increase by a factor of 2 of the thermal neutron flux per unit current, when increasing proton energy from 2 to 2.25MeV. At the time, due to the under-estimation of the dose to patient, it was thought that a proton energy of 2.25MeV could be the optimal choice and Al experiments were initially conducted at this energy. Later, with the possibility of performing more detailed investigations on dose by the means of microdosimetry, it was reported that the dose per unit current increases by a factor of 4.5, while the thermal flux only doubles as energy is increased from 2 to 2.25MeV (Arnold, 2000). The proton energy of 2MeV and a current of 115μA was therefore established as optimal activation protocol, for which the ratio (^{28}Al activity)/(dose to patient) is maximized (Pejovic-Milic, 2001).

The neutron activation procedure in the present project was consequently carried out using these reported parameters. While the investigation or optimization of the activation procedure sits outside the purpose of the present project, it is worth emphasizing that the use of the proposed optimal activation parameters (proton energy and current) in the conditions of a low-performance target had, however, to be done with care. In this respect, it is worth mentioning that previous dose measurements revealed significant discrepancies from the calculated values. Several reasons were anticipated for these inconsistencies (Arnold, 2000), such as: partial loss of proton beam current due to misalignment of beam with the target, loss of lithium due to target melting at high beam currents, etc. Further testing of the different hypotheses lead to the conclusions that Lithium target performance can be affected by inefficient target cooling, and the presence of an oxide layer on target surface (Aslam et al., 2003b).

Because of the variability in time of the lithium target, a means of monitoring neutron fluence rate during the activation of phantoms was necessary for subsequent normalization of each set of data. In the present study, neutron counts were surveyed employing a locally designed long counter. This counter is a BF_3-filled proportional counter wrapped in a cadmium sheet and embedded in a polyethylene moderating cylinder, allowing the detection of higher energy neutrons. The long counter was placed in a fixed position with respect to the accelerator target and in the same conditions (moderator cavity placed in front of the beam) during all experiments. An estimation of the efficiency of the long counter was obtained by calibrating it against an Am-Be neutron source of known activity.

Experiments began with the use of an existing "old" lithium target. Also, the highest proton current attainable by the accelerator at the time was below the optimal proposed value, averaging ~80μA. A portable Anderson & Braun remmeter (Tracelab, MODEL NP-1), commonly called Snoopy, positioned 2m in front of the target, was used to monitor neutron dose. Previous comparative measurements taken with the Snoopy detector for 2MeV at 50cm from the target and a Rossi dosimeter (Arnold, 2000) showed that, on average, the Snoopy reading is 84% of the microdosimetry neutron dose.

Therefore, while it was known that Snoopy underestimates the dose, it could still be used as an indicator of the variations in neutron yield. In the conditions of the existing lithium target, for 2MeV protons and for a current of ~80μA, the Snoopy reading (~200mSv/h) showed a drop of a factor of 2 compared to previously reported values. It was therefore decided to increase the proton energy to 2.25MeV, to adjust for the loss in neutron yield. In the event that the target performance was degraded due to an oxide layer formed at its surface, increasing the energy of the protons at the surface of the target was expected to adjust the neutron yield. As protons are slowed down within the oxide layer, the target atoms will be reached with a slightly smaller energy, closer to the optimal energy value that gives a high thermal flux inside the irradiation cavity. Indeed, for activations at 2.25MeV, the Snoopy reading indicated now between 450-500mSv/h. Since the same range of doses on this remmeter was previously reported (Pejovic-Milic, 1998) for 2MeV and 100μA, it was concluded that no compromise was made with respect to the dose to the patient and a preliminary set of experiments were therefore conducted at 2.25MeV.

It is however worth mentioning that, since the slightest change in proton energy affects the neutron energy spectrum, the choice of irradiation parameters is critical. The ratio of the thermal flux inside the irradiation cavity per dose to patient was no longer at its maximum for 2.25MeV. For assessing the real contribution of the proposed data analysis method, new experiments had to be conducted with a newly prepared and installed Lithium target, when the maximum activation per dose to patient could be achieved for 2MeV proton energy and maximum current.

In-Vivo Neutron Activation Analysis – parameters and procedure

While the majority of the elemental composition experiments by NAA employ whole-body irradiation (Ca, Na, Cl, N, O, P, etc.)(Cohn, 1980), partial irradiation can also present certain advantages. In the case of Al, the main long-term storage organs are thought to be bone mineral (highest levels) and possibly, liver and kidneys (Zafar et al., 1997). Bone is therefore a suitable site of investigation, and knowing that 1.5% of the

skeleton is in one hand (ICRP 23, 1975) if a homogeneous distribution in the skeleton is assumed, the detected quantity of Al in the hand of a patient, for example, can be easily extrapolated to total body Al.

Some of the immediate advantages of Al detection in hand, rather than whole body, are the possibility of achieving a more uniform neutron distribution, given the reduced size of the exposed part, lower attenuation of gamma rays in the soft tissue surrounding the bone, resulting in improved detection, and, most importantly, reduced total dose to patient. Moreover, costly whole body detectors and their associated electronics are no longer a requirement.

A moderating polyethylene cavity for irradiation of a hand was previously designed (Pejovic-Milic, 1998) and is currently employed for thermalization of the neutrons produced from the target. The walls of this cavity are made each of two polyethylene sheets (2x12.6mm thick) and the cavity dimensions are 30x30cm, leaving an interior gap of 9cm, wide enough to accommodate a hand. Besides the need to obtain maximum thermal fluence rate inside the cavity, achieving uniformity of the flux is also important. Ideally, for obvious reasons relating to size, a phantom modeled in the shape of a fist, rather than an open hand, would contribute to preserving flux uniformity during irradiation. However, the enlarged thickness of such a phantom would have the inconvenience of imposing a larger distance between the two NaI detectors used in the gamma ray counting following activation, which would diminish detection efficiency (detection system described in the appropriate chapter). It was therefore decided to pursue with an open hand model for the phantoms, while a real investigation could take place with the patient exposing the fist for irradiation and then the open hand for detection. More recently, with the development within the accelerator neutron activation facility at McMaster University of a new detection system, the phantom shape issue will be eliminated. The new detection system, of higher efficiency, consists of eight NaI detectors with square profile of 10×10×25.4cm, positioned in a well-like arrangement.

The best uniformity of the flux inside the irradiation cavity would be achieved for the cavity located far away from target. However, in our case, the necessity to maximize

the neutron fluence rate onto the phantom required the irradiation cavity to be positioned as close to the target as possible. Physical constraints (electron suppression conductor connected on the external face of the target capsule) restrained the positioning of the cavity to 2.5±0.2cm from target. Inside the cavity, a hand phantom is centered in front of the lithium target (Fig.1).

The irradiation timing protocol was designed based on the short half-live of ^{28}Al (2.25min). Since the activation time is limited by the fast decay, a 180s irradiation interval was proposed as optimal, after which saturation occurs. It is worth mentioning that a shorter irradiation time in the conditions of a higher thermal neutron fluence rate would contribute to achieving a decrease of nearly a factor of $\sqrt{2}$ in the MDL per unit dose.

The irradiation is followed by a 30s transfer time to the counting site, situated outside the accelerator shielded room. The location of the two detectors was chosen such as to prevent the exposure of the NaI crystals to neutrons, but close enough for the transfer time to be reasonably short. A counting time of 5min (~ 2 Al half-lives) was considered sufficient for relatively good statistics.

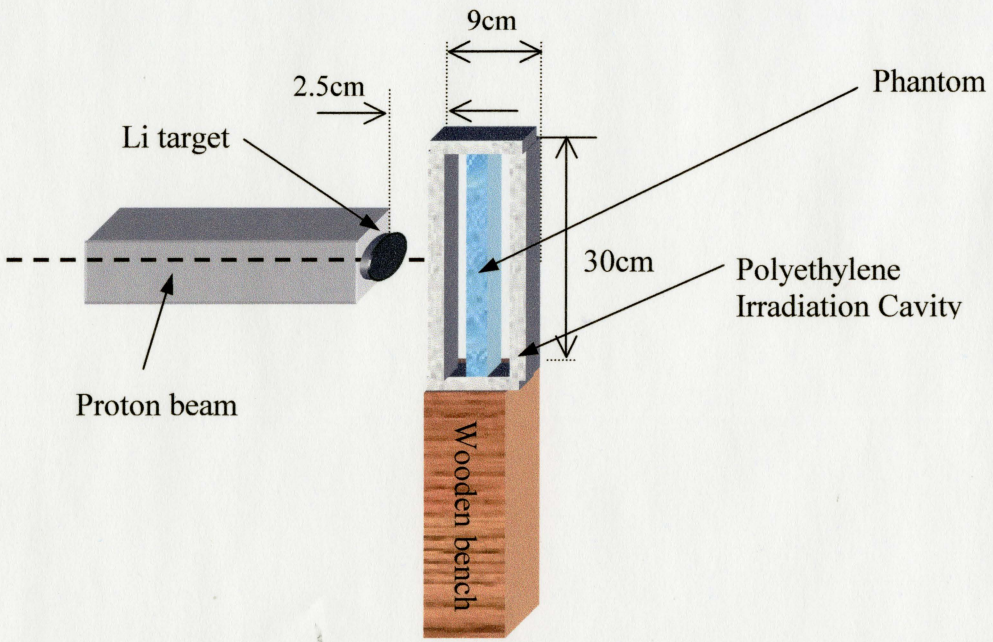

Fig. 1. Accelerator irradiation site. Polyethylene moderator and phantom positioning.

2.2.2. NaI Detection System and Associated Electronics

Detection Method

As stated in the study proposal, a new detection setting was investigated during this project, the electronic rejection of coincidences. Coincidences occur when an isotope emits multiple cascade gamma rays in its decay. In this condition, there is a finite probability that these quanta interact and deposit their energy faster then the detector's response time or the processing time of the electronics. As a result, the gamma rays contributing to the cascade appear as simultaneously detected and a feature known as a *sum coincidence peak* occurs in the spectrum.

The composition of a hand phantom includes two elements for which coincidence detection occurs: chlorine and sodium (Fig. 2.). Therefore, since elimination of single gamma ray by coincidence detection would significantly reduce the smooth continuum to which the Al spectrum is added, the summation effect could be exploited. Al photopeak (1.78MeV) is in close vicinity to one of the two chlorine photopeaks (1.6MeV). By consequence, enhancement of the summation would remove counts from photopeaks, to the benefit of the sum peak, reducing or, ideally, canceling any overlapping of the two photopeaks. This would eventually leave the possibility to fit Al peak using a single Gaussian curve.

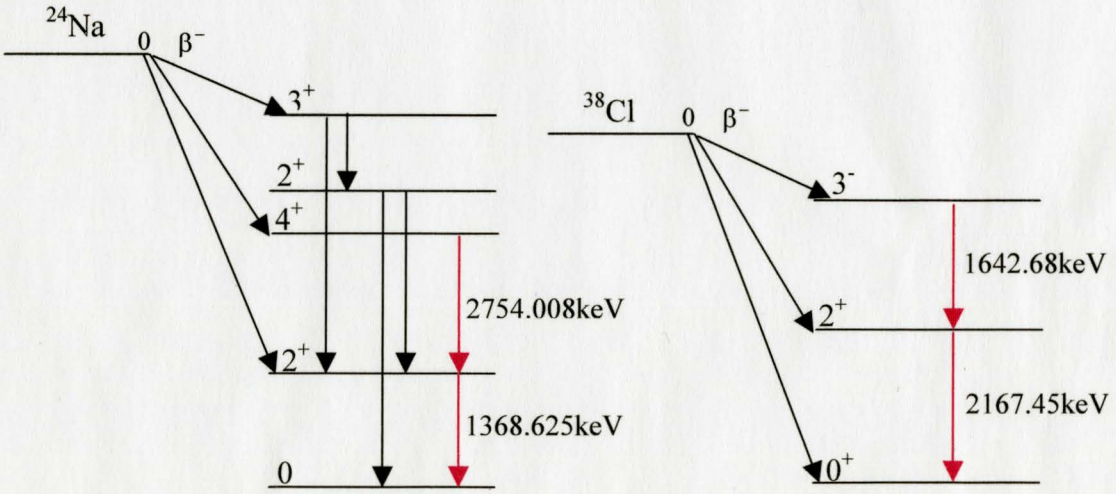

Fig. 2. Illustration of cascade decaying corresponding to ^{24}Na and ^{38}Cl.

The detection of a pair of cascade gamma rays, say γ_1 and γ_2, originating in a source of strength S, by two detectors in an arrangement similar to the one sketched below, would happen as follows: the number of counts in detector A, originating from γ_1, and without the detection of its pair ray in any of the detectors, is given by N_{A1} (Eq.1). Similarly, for detector B and for the same gamma ray, a number N_{B1} of counts is obtained (Eq. 2).

$$N_{A1} = \varepsilon_{A1} \cdot (1 - \varepsilon_{A2} - \varepsilon_{B2}) \cdot S \quad (1)$$

$$N_{B1} = \varepsilon_{B1} \cdot (1 - \varepsilon_{A2} - \varepsilon_{B2}) \cdot S \quad (2)$$

The total rate due to γ_1 gamma-ray, in the absence of coincidences, is then:

$$N_1 = N_{A1} + N_{B1} = (\varepsilon_{A1} + \varepsilon_{B1})(1 - \varepsilon_{A2} - \varepsilon_{B2}) \cdot S \quad (3)$$

When coincidences are detected, the number of counts that form the sum peak is given by:

$$N_\Sigma = (\varepsilon_{A1}\varepsilon_{A2} + \varepsilon_{A1}\varepsilon_{B2} + \varepsilon_{B1}\varepsilon_{A2} + \varepsilon_{B1}\varepsilon_{B2}) \cdot S \quad (4)$$

Practically, coincident events can only be detected if each gamma ray of the cascade pair enters a different detector. Therefore, of the total coincidences, the number that cannot be electronically eliminated is given by equation (4), in which cross terms are removed:

$$\overline{N}_\Sigma = (\varepsilon_{A1}\varepsilon_{A2} + \varepsilon_{B1}\varepsilon_{B2}) \cdot S \quad (5)$$

If the two detectors are taken as identical, which is often the case, equation (3), (4) and (5) further reduce to:

$$N_1 = \varepsilon_1(1-\varepsilon_2)\cdot S \qquad (3')$$

$$N_\Sigma = \varepsilon_1\varepsilon_2 \cdot S \qquad (4')$$

$$\overline{N}_\Sigma = \frac{N_\Sigma}{2} \qquad (6)$$

Because nothing can be done about those events in which both gamma-rays interact with the same detector, eliminating coincidences only reduces the sum events by a factor of two (Eq.6).

Elimination of coincidences from the original spectrum can be electronically achieved by their routing to a secondary spectrum. A coincidence unit was specially designed for this purpose. Consequently, the subtraction of the obtained secondary spectrum, in which half of the total number of coincidences is expected, from the original spectrum containing the remaining half of the coincidences, will ensure complete clearance of coincidences from the spectrum.

Since detector events occur at random times, besides the true coincidences, accidental coincidences (*chance coincidences*) of two separate events from independent decays can also arise in the coincidence counting. To reduce accidental coincidences one should make the resolving time as small as possible. However, the resolving time cannot be reduced below a certain value without losing true coincidences, so the type of detector determines the minimum resolving time usable. Fortunately, in the present experiment no significant random adding was observed.

NaI Detectors

Examining Eqs. (3') and (4') one can see that good detection efficiency is crucial when using the proposed approach. Eq. (3') shows that ideally, when $\varepsilon_2 \to 1$, $N_1 \to 0$, so that all the counts are removed from the photopeak. One strong reason motivating the choice of NaI detectors over germanium semiconductor detectors was therefore their

much higher detection efficiency. Also, factors like availability, cost, maintenance (*e.g.* liquid nitrogen) were considered.

It is the high Z of iodine in NaI that makes these scintillating detectors highly efficient for gamma-ray detection. A gamma ray interacting with a NaI crystal produces a pulse of light, with a typical decay time constant of about 0.23μs (Birks, 1964). Photomultiplier tubes convert the flashes of light into an electrical signal, whose integrated area is proportional to the number of photons in the flash of light. The photomultiplier consists of a photocathode, a focusing electrode, and several multiplying dynodes. The anode and dynodes are usually biased by a chain of resistors typically located in a plug-in tube base assembly.

Investigations were conducted for choosing the most efficient detection equipment available within the facility. Two pairs of NaI detectors were therefore investigated: a larger diameter set, but with a thinner crystal (200x50mm) versus thicker but smaller diameter ones. Solid angle versus thickness trade-off with respect to efficiency improvement turned out to be in favor of larger diameter detectors. It was therefore decided to keep the two cylindrical NaI detectors (200x50mm) that have also been used in previous studies (Pejovic-Milic, 1998, 2001). Also, the same detection arrangement was used, with the two detectors facing each other in a quasi-4π geometry. The space between the detectors was adjusted to 4.5cm. A wider gap could compromise the detection efficiency, but at the same time, the width has to be large enough to accommodate the patient's hand in the view of *in-vivo* measurements. Maximization of signal-to-noise ratio required the confinement of the detector assembly in a lead box, made of 6cm thick lead bricks. Lead considerably shields background radiation (K, Th, high-energy cosmic rays, etc.) from interfering with the signal of interest.

Moreover, during experiments involving the use of accelerator, it was discovered that a considerable amount of thermal neutron radiation was reaching the iodine in the detector crystals, inducing its activation. The corresponding reaction is:

$$^{127}\mathrm{I} + \mathrm{n}_{\mathrm{th}} \rightarrow {}^{128}\mathrm{I} + \beta^{-},\ E_{\beta^-} = 2.118\mathrm{MeV}$$

As indicated, this reaction is accompanied by emission of beta radiation, resulting in a continuum that overlaps with the spectrum of interest. As further explained in the results chapter, a neutron shield consisting of a wooden box lined with 0.5mm boronated polyethylene sheets had to be built to prevent neutron activation of the detectors.

An inconvenient feature in using NaI detectors is their rather unstable gain that results in respective peak shifts in the spectrum. This is thought to be mainly caused by temperature and/or count rate variations. As is common for most scintillators, the light yield per unit energy deposition decreases with increasing temperature in NaI(Tl). For a typical three-inch diameter by three-inch deep crystal, one might expect an approximately linear drop in light output of about 0.15 to 0.2% per degree centigrade in the interval from 20° to 180° (Birks, 1964). The decrease in light yield with increasing temperature varies with the physical dimensions of the NaI(Tl) crystal. Knoll (Knoll, 2000) suggests that this may be due to differences in surface reflectivity among crystals. During the present experiment, of a relatively short duration (~2h), we expect temperature variations in this interval to be negligible. Temperature was monitored with a regular room thermometer and no variation bigger then 0.5° was noticed.

In the case of high count rate samples, the voltage on the resistors biasing the dynodes in the photomultiplier can decrease because of the detection of high currents, inducing gain shifts. The extent of this phenomenon for our detection system was investigated using three ^{232}Th sources of different activities. Significant shifts of up to 70keV (~7 channels) for the highest activity source were observed. However, this problem was easily maintained under control by choosing suitable parameters for the irradiation of the samples, so that the count rates did not vary significantly from one experiment to another. On the long term, it was suggested to address this problem by replacing the regular resistors in the photomultiplier tubes with stable Zener diodes.

Before each experiment, a ^{232}Th source was used for matching the gains on the two detectors. The 2.6MeV peak of ^{232}Th was a convenient choice, given the range of energies covered in the spectrum.

Electronics set-up

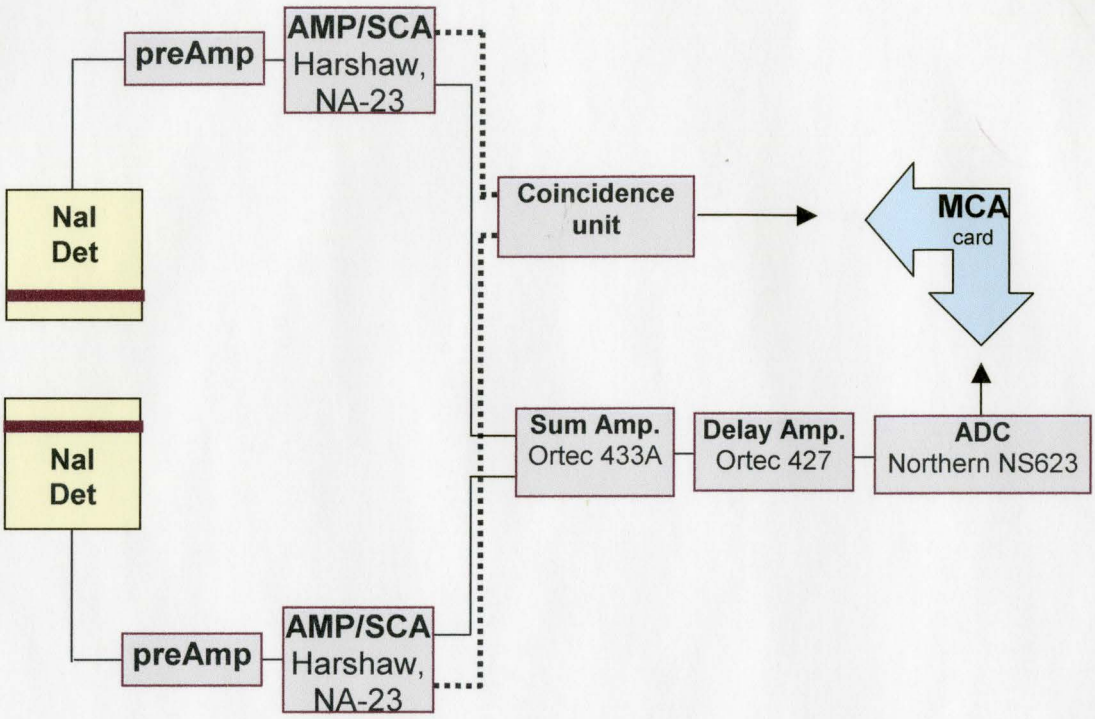

Fig.3. Electronics set-up.

Four photomultiplier tubes are connected in parallel on each detector. As the output of the photomultiplier is a charge pulse proportional to the gamma-ray energy, a preamplifier converts this to a voltage pulse using a capacitor (V = Q/C). The pulse rise time, important for timing measurements, is dependent upon the scintillation decay time and on the collection and transit time characteristics of the photomultiplier tube. The signals are then passed by two combined amplifier/single-channel-analyzer systems (Fig.3). Bipolar shaped signals are used. Besides the amplification function, this unit shapes the pulse for an optimum energy resolution. In addition, the decay time of the pulse is much shorter than after the preamplifier, preventing overlap (pile-up) of pulses in high-count rate experiments.

The SCA output of each amplifier is then fed into a coincidence unit. The logic output pulse of a SCA carries a definite time relationship to the linear pulse that caused it.

The coincidence circuit passes the resultant sum pulse through a discriminator level and generates an output pulse when the two input pulses overlap. The period of time in which the two input pulses can be accepted is defined as the resolving time and is determined by the width of the pulses, τ, such that the resolving time is equal to 2τ. More specifically, in our case, the unit produces a pulse when the leading edges of the enabled logic inputs occur within the set resolving time. In this experiment, the resolving time was set to a typical value of 30ns.

The linear outputs of the two amplifiers are summed and the sum signal is passed through a delay amplifier before being fed into an ADC unit. The sum amplifier output goes to the ADC with a delay of 1.5μs and it is then directed to the MCA card located in a personal computer. The logic signal coming from the coincidence unit meets the sum signal in the MCA, so that the coincident and non-coincident pulses are each stored in separate 512-channel memory areas. Locally designed software was used for data acquisition.

2.2.3. Phantom composition

A first set of measurements was taken using a readily available set of 6 phantoms, which were manufactured and used for a previous Al project (Pejovic-Milic, 2001). This experimental part intended to confirm the reproducibility of the irradiation technique, estimate the coincidence counting setting performances, and verify the decomposition analysis algorithm. These were 22x12x2.5cm phantoms confined in a resin matrix. The zero-concentration phantom was found to be contaminated due to Al traces in the resin, so that new phantoms had to be made.

Along with the phantoms, in the course of this project, single element solutions, referred to as "standards", were required by the proposed data analysis technique. Irradiation and counting of these standards in the same conditions as the phantoms provided a library of specific detector response functions for the elements that constitute the phantoms. The three elements contained in the bones and soft tissue of the hand that are most responsive to neutron activation are: Ca, Cl, Na. In addition, an Al standard provided the same information for the investigated element. Since perfect matching of the response functions with the phantom spectra is finally desired in the view of analysis by spectral decomposition, the standards had to have exactly the same scattering and attenuating properties as the phantoms. Identical materials and dimensions were therefore used for standards and phantoms.

In investigating the MDL, phantom purity becomes essential. Water solutions of the chemical constituents of the hand and wrist were therefore proposed, and were used both for standards and for the phantoms. Methyl methacrylate (Lucite) holders for the water solutions are considered as accurate models of the human skin and soft tissue. Rectangular Lucite holders of 20x10x2cm, enclosing a volume of 350ml, were manufactured and their purity was tested by irradiation of blank phantoms.

Even with the aid of an extensive library of chemical composition data published by ICRP 23, establishing an accurate composition for the hand and wrist was challenging. The available information was most accurate on bone composition, while the soft tissue

contents were arrived at based on the assumption that the percentage by weight for each element of total body soft tissue is the same in the hand and wrist, as the bone percentage of the total skeleton. However, comparison of the spectra obtained from the phantoms employed in this study with published spectra recorded during clinical applications on patients (Wyatt *et al.*, 1993) confirmed the accuracy of elemental composition of our phantoms.

There is also the dynamical aspect of the model, being known that the blood content of a hand and wrist is replaced by pumping every ~30s, that could not be included in the present study. However, in the case of a clinical application, this will work in model's favor, since part of the radioactive sodium and chlorine in the hand blood would be replaced with their stable isotopes by the time the irradiated hand is counted.

The final composition of the phantoms, along with the used chemical compounds, is given in Table III. Phantoms with a total volume of 380ml, containing an increasing amount of Al (0, 2, 5, 10, 20mg) were investigated.

Table III. Phantom composition.

element	Hand and wrist composition* (g)	Used chemical compound (g)
Ca	14.9	88 $Ca(NO_3)_2$
Cl	1.19	1.962 NaCl
Na	1.25	1.766 $NaNO_3$

*Quantities calculated assuming 1.5% of the skeleton in one hand (ICRP 23, 1975)

2.3. Data Analysis

Library-oriented fitting

The fitting approach used in this project, spectral decomposition analysis, is based on the simple principle that the gamma-ray spectrum of a sample is the superposition of spectra from all the radioactive isotopes in that sample.

A new library-oriented fitting routine, developed in Fortran, was designed for the specific aspects of spectral decomposition analysis. Within this routine, the contributions from each isotope are summed with varying intensities until the best fit between the experimental and model spectrum is obtained. A least-squares method was used for comparing the data with the model and the minimum value of the reduced Chi-squared function indicates an optimal fit. In reality, the least-squares method derives from the more general principle of maximum likelihood. If $\mathcal{P}(N_i, \boldsymbol{\alpha})$ is the probability density function for a collection of N_i counts in channel i (i=1,N), where $\boldsymbol{\alpha}$ is a vector of fitting parameters, the likelihood function is given by $L = \ln \prod_{i=1}^{N} \mathcal{P}(N_i, \boldsymbol{\alpha})$ and it has a maximum for $\frac{\partial L}{\partial \alpha_k} = 0$. The counting distribution, $\mathcal{P}$, is a binomial, but for processes with small and constant success probability (*e.g.* observation time small compared to the half-life of the source, small efficiencies, etc.) it becomes a Poisson distribution. Moreover, for expected mean values >12, the Poisson distribution can be approximated by a Gaussian, and $\mathcal{P}$ becomes:

$$\mathcal{P} = \frac{1}{\sqrt{2\pi} \cdot \sigma_i} \exp\left(-\frac{(N_i - \overline{N}_i)^2}{2\sigma_i^2}\right),$$

where $\overline{N}_i$ is the model estimate and σ_i^2 is the predicted variance of the distribution. The likelihood function is then:

$$L = \sum_{i=1}^{N} (\ln \frac{1}{\sqrt{2\pi} \cdot \sigma_i} - \frac{(N_i - \overline{N}_i)^2}{2\sigma_i^2})$$

and reduces to: $L = C - \frac{1}{2}\chi^2$. The first term is therefore a constant (C) and setting $\frac{\partial L}{\partial \alpha_k} = 0$ is equivalent to the reduced Chi-squared method ($\frac{\partial \chi^2}{\partial \alpha_k} = 0$). Consequently, the use of the least-squares method in the present fitting routine is legitimate.

It is also worth mentioning that this fitting routine is linear, unlike the more commonly used Gaussian fittings, which are nonlinear (*e.g.* Marquardt method). While a nonlinear fitting gives more flexibility, its increased number of variables also increases the uncertainties in the fitting parameters, which is a major disadvantage when estimating MDL. One of the benefits of spectral decomposition analysis is therefore a reduction in the number of fitting parameters. However, the most important advantage of the method resides in the recovering of an increased number of counts that are specific for a certain element. As mentioned in the study proposal (section 2.1.), spectral decomposition analysis uses the complete detector response to the energies and characteristics of each element in the spectrum, rather than only the information contained in the photopeak. Since the MDL of a technique is ultimately proportional to the inverse of the square root of the number of counts, the proposed method should lead to improved sensitivity. The degree of improvement depends on the photopeak-to-total ratio in the spectrum, which is in turn related to the efficiency of the detection system.

Since a gamma-spectrum is the "fingerprint" of each decaying nucleus, the detector response to each of the contributing elements was experimentally obtained by collecting single-element standard spectra. Particular care was given to acquiring spectra with good statistics. To account for all the different features in the combined spectrum, the experimental conditions were kept unchanged when collecting the standard spectra and the spectra from phantoms. Apart from the three major elements that form the spectrum of a hand, Al and background spectra were also introduced in this library as fitting variables, raising the total number of variables to five (Ca, Cl, Na, Al,

background). The presence of the Ca peak in the spectrum of a hand is an important aspect, providing a means of normalizing the data. During a clinical investigation, Ca response depends on the amount of bone in the hand, the neutron field profile (variable, depending on target performance), and the irradiation and counting geometries. Since Al response also depends on the same factors, the ratio of Al to Ca provides a reliable means of determining Al concentration. This ratio is independent of the geometry and experimental conditions.

Fortran fitting routine

Once a library of standards was established, the probability of detecting one count per channel was calculated for each of the five standard spectra. The probabilities per channel for each element were then used to generate a single probability matrix for the fitting routine.

Let p_{ij} be the probability of isotope *j* contributing a count in channel *i*. Then a model of the observed spectrum is given by:

$$m_i = \sum_{j=1}^{K} p_{ij} \cdot c_j ,$$

where c_j (j=1,K) represents the relative contribution of the isotope *j* and constitutes the desired information. For our particular case, K=5 is the number of fitting variables and N=512 is the total number of channels. In matrix form this may be written as:

$$\mathbf{m}=\mathbf{P}\cdot\mathbf{c} ,$$

where **m** is a Nx1 column vector, **P** is a NxK matrix and **c** is a Kx1 column vector.

Let **d** be the Nx1 experimental data vector. For the best fit, the Chi-squared function:

$$\chi^2 = \sum_{i=1}^{N} \left(\frac{1}{d_i}\right) \cdot \left(d_i - \sum_{j=1}^{K} p_{ij} \cdot c_j \right)^2$$

should be minimized with respect to c_j, $\frac{\partial \chi^2}{\partial c_j} = 0$. This finally leads to:

$$\mathbf{c} = \mathbf{Design}^{-1} \cdot \mathbf{v},$$

where $\mathbf{Design} = \sum_i p_{ki} \cdot p_{ji} / d_i$ is a KxK matrix and **v** is the Kx1 identity matrix, with the j^{th} element $v_j = \sum_i p_{ij}$.

In order to calculate the isotopic contributions c_j, the addition of a matrix inversion sub-routine in the fitting program was required. The elements of the inverse matrix $\mathbf{Design}^{-1}$, also called "error" or "covariance" matrix, are the variances and covariances of the fitted parameters c_j.

The second approach to fitting analysis was to include the known information on the time dependency of the spectra. For this purpose, the input data file for the experimental spectrum was made of a series of three spectra, instead of a single spectrum. The spectra were collected at specific time intervals $r\Delta$, [r=0,2; Δ=150s] and data were read in by the program as a 3Nx1 column vector, where N is the total number of channels for a spectrum acquisition. For the time dependent approach, the Chi-squared function becomes:

$$\chi^2 = \sum_{i=1}^{3N} \left(\frac{1}{d_{(r\cdot N+i)}}\right) \cdot \left(d_{(r\cdot N+i)} - \sum_{j=1}^{K} p_{ij} \cdot e^{-\lambda_j \cdot (r\cdot\Delta)} \cdot c_j \right)^2,$$

where λ_j is the decay constant for isotope j.

Following the derivation of the c_j parameters, the reduced Chi-squared eventually gives a measure for the goodness of the fit. To account for the goodness-of-fit, the variance of the fitting parameters were in each case corrected for the reduced Chi-squared:

$$\sigma'^2 = \sigma^2 \cdot \frac{\chi^2}{\nu},$$

where σ^2 is the uncorrected variance given by the inverted design matrix.

Since the ultimate aim of the project is to increase method's sensitivity, and given that the MDL depends directly on the standard error in a zero concentration phantom, a correct estimation of the variances is essential. The fitting algorithm was therefore tested in the following manner. Data was simulated by combining the probability matrix with a known vector. Using a random number generator, noise was added to the simulated data. By running the application a number of times (~100) it was possible to calculate the variance of simulated data and compare it to the average of the computed variances, given by the fitting routine. The comparison was made by plotting simulated versus computed variances. The graphs were then fitted with linear functions ($y=ax+b$) and ideally, a zero intercept and unit slope would confirm that the computed and simulated variances are equal. As expected, the obtained parameters proved the success of the Fortran fitting routine. A sample graph of the testing procedure result is reproduced below.

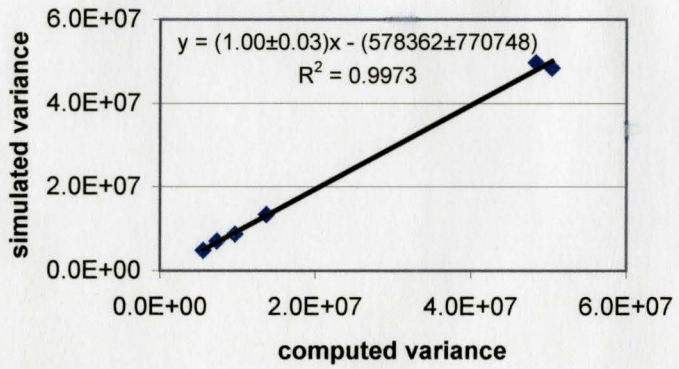

Fig. 4. Example of fitting routine testing: the variances of the six fitting parameters, calculated for 20 sets of simulated data, were in good agreement with the computed variances, returned by the fitting routine.

MDL calculation

The MDL of a system is defined as the minimum concentration of an investigated sample that can be distinguished from a concentration of zero. The common expression for the MDL used in the field of *in vivo* body composition measurement is:

$$\mathbf{MDL} = \frac{2 \cdot \sigma_0}{(\text{calibration slope})}$$

(O'Meara, 1999; Pejovic-Milic, 2001; Arnold, 2000), where σ_0 is the uncertainty in the zero concentration phantom, and the calibration slope is obtained by plotting the ratio Al/Ca of the fitting parameters c_j, versus the Al content in grams of each phantom. The MDL will therefore express the minimum detectable amount of Al in grams. The comparison of detection systems based on the MDL alone may be misleading, as the improved detection limit may be at the expense of the total dose delivered to the patient during the measurement. In this project, the MDL will therefore be reported in conjunction with administered dose to the hand.

The standard deviation in the MDL value was assessed from propagating the uncertainties based on the MDL calculation formula. As previously stated, the error in the calibration line slope is calculated by linear regression analysis weighted with the standard deviations of the data. The uncertainty in the standard deviation corresponding to the zero concentration phantom was derived based on the standard deviation of the F distribution. A common statistical procedure for comparing the variances of two population is the "F test", which is based on the F distribution function (Bevington, 1993). The variance of the F distribution is given by:

$$\sigma_F^2 = \frac{2\nu_2^2(\nu_1+\nu_2-2)}{\nu_1(\nu_2-2)^2(\nu_2-4)}, \quad \nu_2 > 4,$$

where ν_1 and ν_2 are the degrees of freedom of the two distributions to be compared. In our case, an absolute estimation of the uncertainty in the variance of one distribution is needed. Imposing that the second distribution has an infinite number of degrees of freedom ($\nu_2 \to \infty$), σ_F^2 approaches the variance of a distribution with ν_2 degrees of freedom and its square-root is the sought after percent uncertainty. Therefore, when $\nu_2 \to \infty$, $\sigma_F^2 \to \frac{2}{\nu_2}$. The standard deviation in the zero concentration phantom may be written as:

$$\sigma_0 \pm \sqrt{\frac{2}{\nu_1}} \cdot \sigma_0 ,$$

where ν_1=345 is the number of degrees of freedom in our data, given by the total number of channels over which the fitting was executed (350) minus the number of fitting variables (5). This results in a 7.6% percent error in the obtained standard deviation. Correlating this with the 2.5-3.5% error in the calibration line slope, a percent error in the 16-18% range was estimated for the MDL values reported in this project. This evaluation is consistent with the experimental uncertainty of 20% in the MDL reported by Arnold (Arnold, 2000) in an IVNAA study of manganese, calculated over three experimental trials.

Chapter 3. Results and Discussions

The experimental pursuit started with the testing of the coincidence unit and, implicitly, with the performance evaluation of the proposed approach. A standard Co-60 source was used for this purpose. Co-60 decays through the emission of two gamma rays occurring in cascade (1.173 and 1.332MeV) and was therefore suitable for this investigation.

From the technical point of view, the rejection of coincidences from the main spectrum was successfully achieved. However, due to the low efficiency of the NaI detectors used, only a small fraction of the coincidences could be detected. For the characteristic gamma ray energies of Co-60, the detection efficiency was estimated to be 54%, resulting in a sum-peak/photopeak ratio of 0.2. Overall, the technique did not prove valuable within this experimental context, but with an improvement in detection efficiency, its potential could be exploited. A new detection system consisting of 8 NaI detectors in a well-like arrangement was recently built within the facility. Its efficiency of 96% greatly exceeds that of the current

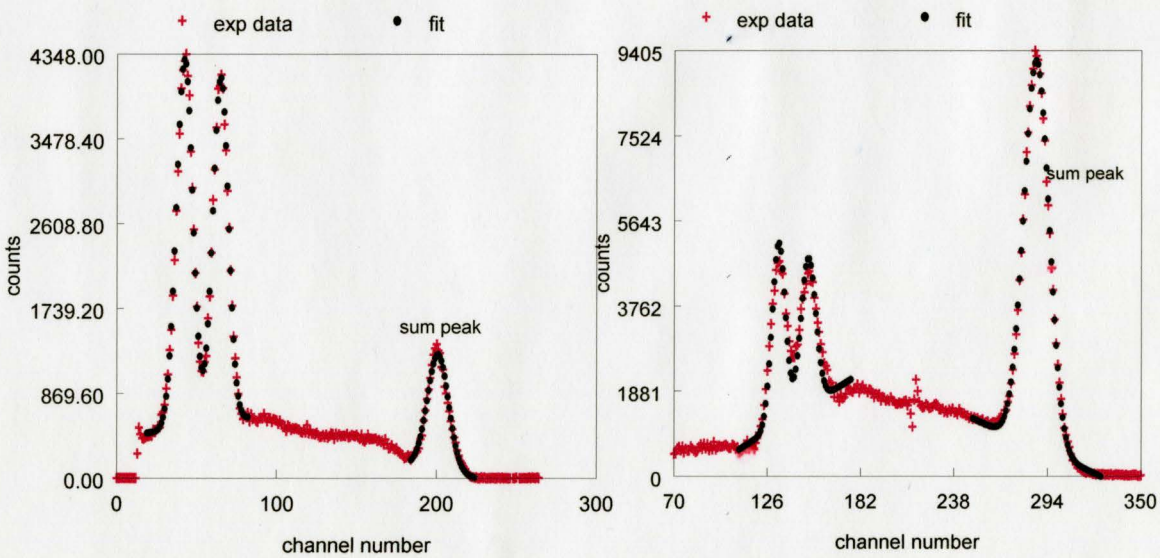

Fig. 5. The ratio sum peak to photopeak in a Co-60 spectrum increases by a factor of 10 when using 8 NaI detectors in a well-like arrangement, compared to the 2 NaI detection system.

system and the detection of coincidences is increased to a sum-peak/photopeak ratio of 2. As can be seen from Fig.5, the new system shows promising results and its performance will be investigated as part of a different project.

A. Resin phantoms were used for the first set of measurements, intended as a validation of the new data analysis procedure and of the fitting routine. Also, the experimental practice for the irradiations established by the former studies on Al at McMaster had to be implemented. The already available hand resin phantoms had been previously used for a Manganese detection study (Pejovic-Milic, 2001), and therefore contained Manganese. A Mn standard was hence included in the library of the fitting routine, along with the Al, Ca, Na, Cl and background standards. However, with the manufacturing of new higher purity phantoms and since Manganese would only occur in a very small concentration in the hand, this standard will no longer be used for other experiments.

Five Lucite containers of dimensions 6X6X2cm were manufactured as holders for the single element standards and were then pre-tested for impurities. A blank phantom, together with the sealing tape, was irradiated and counted following the implemented protocol. The collected spectra showed no measurable amounts of impurities.

In this first experiment, powder compounds of Al, Ca, Na, Cl and Mn were irradiated in the reactor facility. This was necessary in order to obtain reasonably high activity standards, which would then allow the collection of standard spectra with very high statistics. The active powders were then dissolved in water, diluted HCl or HNO_3, to a volume that completely filled the Lucite holders. The holders were then sealed, transported to the detection system site and counted for suitable time intervals.

The obtained standard spectra were then tested for pile-up effects by monitoring the peak shapes in spectra taken at different time intervals. No pile-up effect was noticed. Furthermore, irradiation of standards in the reactor predicts the occurrence of different isotopes from neutron threshold reactions. For the neutron energy spectrum of the accelerator, these threshold reactions cannot take place and therefore the response functions of the detectors to elements irradiated in reactor could differ from those

irradiated in the accelerator. Fortunately, when analyzing the standard spectra, no fast neutron reaction products were identified and the standard spectra were considered suitable for the proposed fitting procedure. Also, later during the investigations, these standards were compared to a set of standard spectra acquired by irradiation using the accelerator and their similarity was again confirmed.

However, the irradiation protocol was later reviewed and it was decided that activating the standards in the accelerator would lead to count rates comparable to those of the irradiated phantoms. Similar count rates for standards and phantoms ensure a better stability of the NaI detector gains. For achieving spectra with good statistics, extended counting of the standards was considered, or, in the case of short-lived isotopes, an increased amount of sample compensated for the shorter counting time.

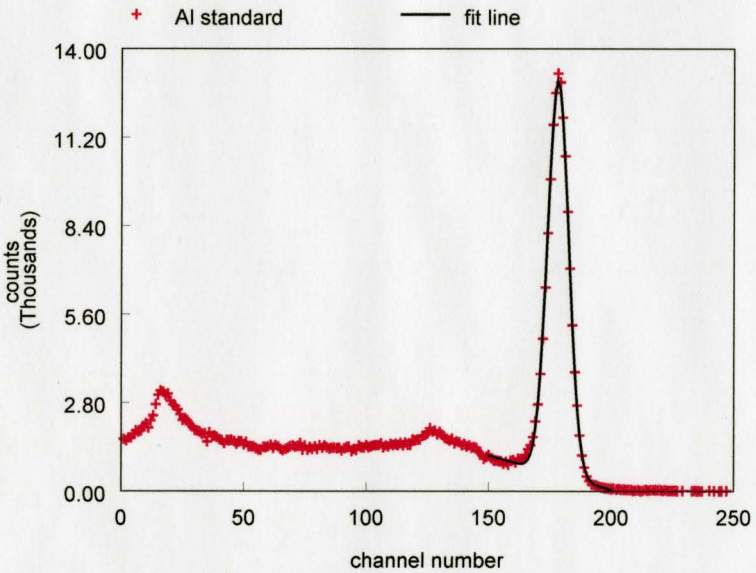

Fig. 6. Al standard: peak-to-total ratio 0.32.

Once the Al standard spectrum was obtained (Fig. 6), the expected improvement factor in the MDL was calculated. The peak-to-total ratio of 0.32 indicated that an improvement factor of ~1.7 could be achieved in the MDL when spectral decomposition is used as an alternative to data analysis based on the photopeak area. Six different

spectral contributions, from the five elements in a hand phantom plus the background, convolve to the model spectrum used by the fitting routine, as shown in Fig.7.

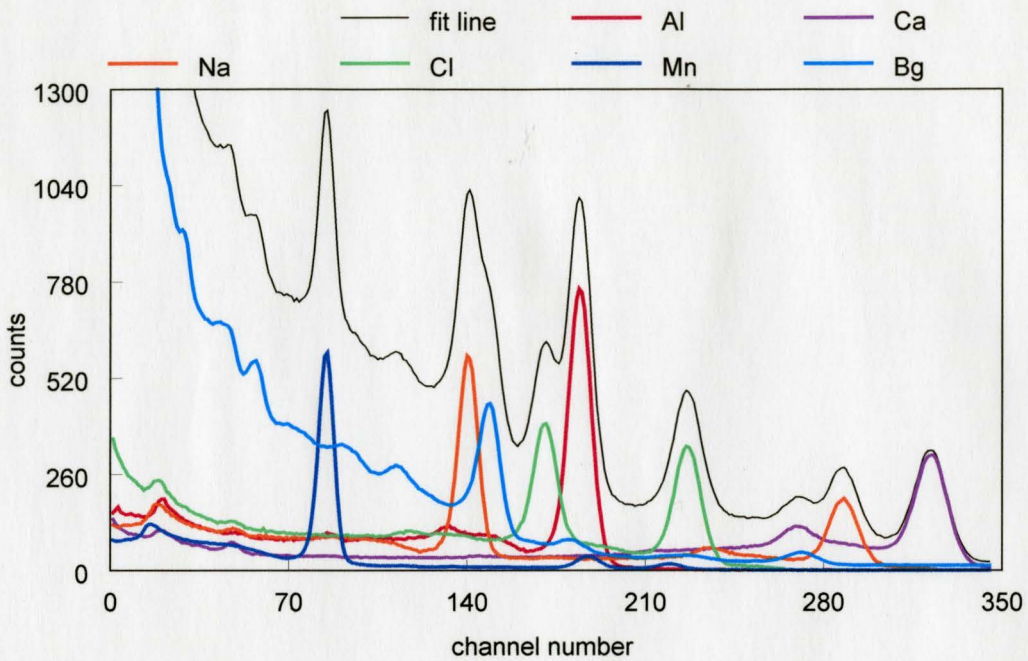

Fig. 7. The six spectral components of a model spectrum.

For the irradiation of the phantoms a 2MeV proton beam was accelerated onto the lithium target. The maximum achievable proton current was used, its value averaging 90μA. However, the current on the third Faraday cup on the beam line, which should be equal or slightly higher than the true value of the current on target, indicated only 70μA. As pointed out earlier, this confirms that the target current reading was only reliable within approximately 20%. During the irradiations, the Snoopy detector was kept at the standard position (aligned with the beam, 2m from target) and, for the given proton current, its reading was within 45-50mRem/h. The phantoms were irradiated for 180s each, transferred to the counting site in 25-30s, and counted for 300s. During the counting, the MCA recorded 15-20% deadtime. The fitting routine based on spectral

decomposition was subsequently tested on the acquired spectra. Fig. 8 presents the experimental spectrum for a hand phantom containing 20mg Al and its corresponding model spectrum.

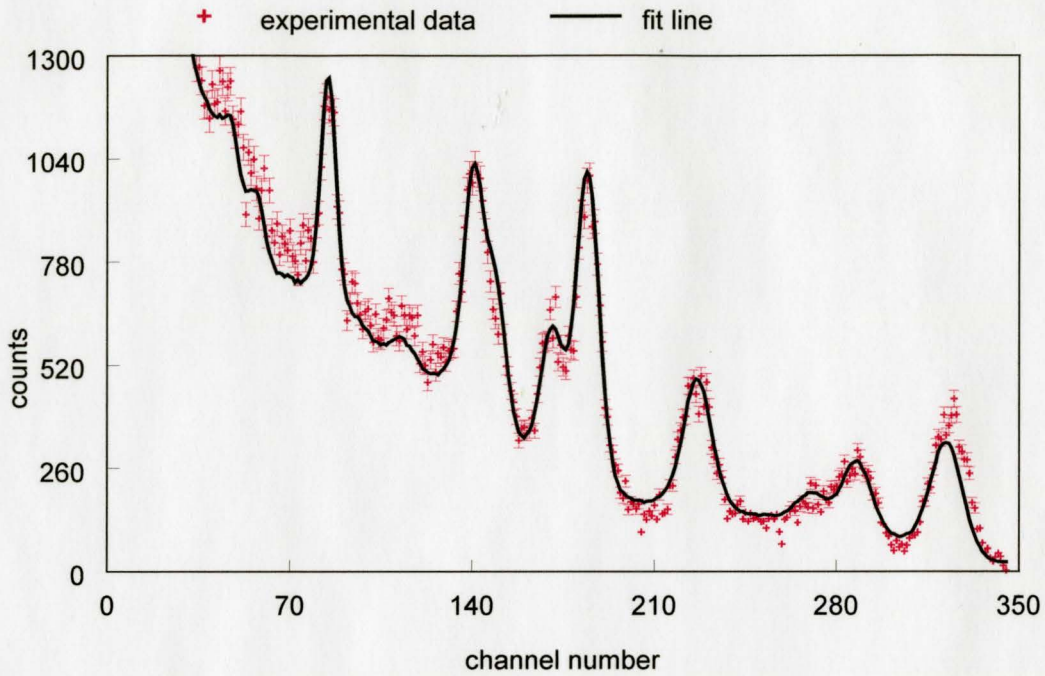

Fig. 8. Example of fitting on a resin phantom spectrum containing 20 mg Al ($\chi^2/\nu = 6$).

From Fig. 8 one can see that the model failed to closely reproduce the experimental data in the low energy region of the spectrum. The reduced Chi-squared values, in the 5 to 6 range, also indicated a poor goodness-of-fit. It was later investigated and found that the discrepancy in the low energy region was mainly due to an unaccounted for contribution to the spectrum. Fast neutrons penetrating the accelerator room walls were activating ^{127}I in the NaI detectors ($^{127}I + n_{th} \rightarrow {}^{128}I + \beta^-$). Given the large amount of iodine in the detector crystals and the high cross-section of iodine for thermal neutrons ($\sigma_c = 6.1b$), the activation was not negligible. The emission of beta particles with energy $E_{\beta^-} = 2.118MeV$ resulted in a continuum that overlapped with the spectrum of

interest. It was therefore necessary to shield the detectors in order to prevent iodine activation, which would ultimately lead to improvement of the fitting.

A neutron shield consisting of a wooden box lined with 0.5mm boronated polyethylene sheets was built. Figs. 9 a) and b) present background spectra acquired before and after enclosing the detectors with the neutron shield. The first spectrum (red line) was acquired while the accelerator beam was on target and neutrons were being produced. The second and the third spectra (dark and light blue lines) were collected immediately after the accelerator was shut down and 33 minutes after that, respectively. A background spectrum (black line) acquired after the iodine had completely decayed is shown for comparison. Fig. 9b) illustrates the almost complete removal of activation in the presence of the neutron shield (compare blue and black spectra).

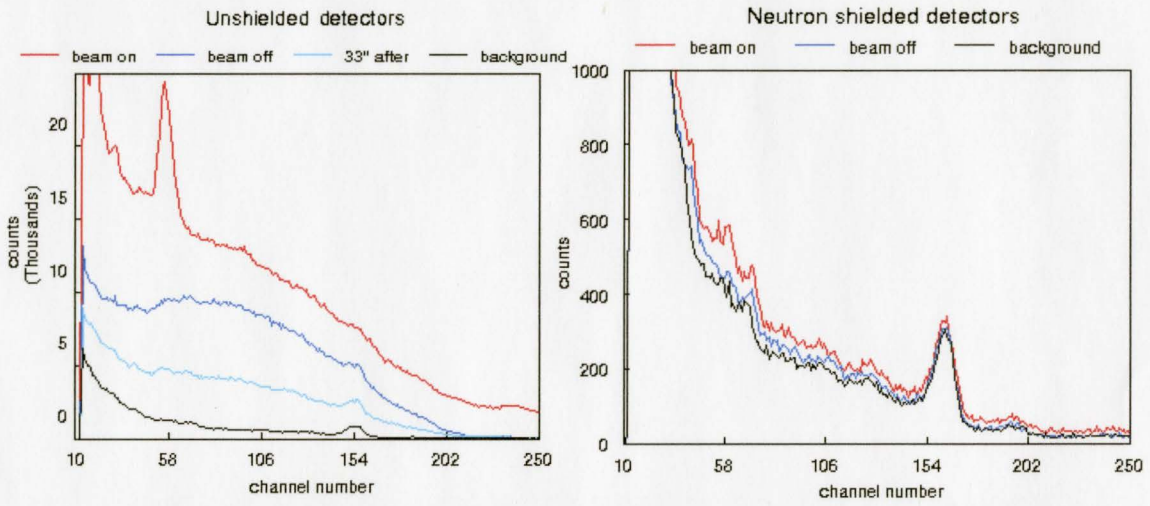

Fig. 9. Background spectra acquired at different time intervals during and after accelerator operation. a) unshielded detectors. b) neutron shielded detectors.

Different attenuation properties of the phantoms compared to the standards, due to differences in size (the phantoms are two times thicker than the standards) and composition (resin vs. water solutions), may have also contributed to the poor fitting of these spectra. In the low energy region, an enhanced Compton effect in the case of phantoms with respect to standards may be responsible for the obvious worsening of the fitting. Another aspect that may have contributed to deteriorated fitting was the slight misalignment of standard and phantom spectra, due to the unstable gains on the NaI

detectors. As detailed in the methodology section, gain shifts can originate from the NaI crystals, induced by the temperature dependence of the light yield per unit energy deposition, or from the photomultipliers, as a result of count rate variation. Because of the long acquisition time required for good statistics in the background spectrum, there was a higher probability for gain shifts to occur while counting the corresponding standard. It was indeed noticed that the potassium peak in the background standard recurrently underwent shifts of up to 3 channels. The correct position of the K peak was derived from an energy calibration line obtained using the centroid of each peak in the standard spectra (Fig. 10), and subsequently, the detector gains were adjusted for that position. The energy calibration line further allowed for a routine inspection of the detector gains at the beginning of each experiment.

Also, gain shifts had been noticed in cases where no considerable depreciation of peak resolution occurred. An occasional malfunctioning of the summing amplifier was therefore suspected.

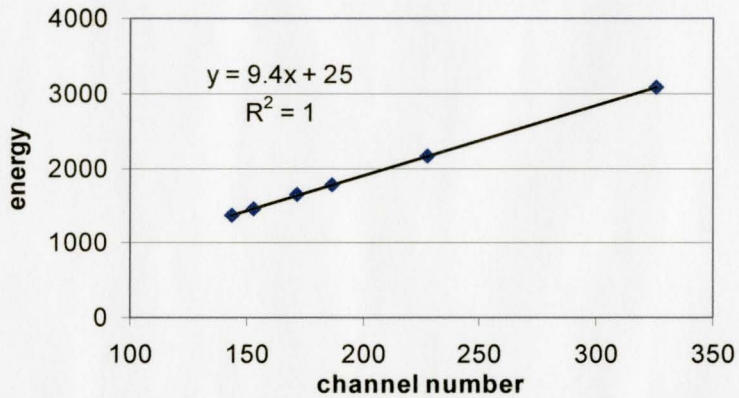

Fig. 10. Energy calibration line used for standard spectra alignment.

Table IV summarizes the contributions of Al/Ca in each of the six investigated phantoms, as given by the fitting parameters. The slope, intercept and associated errors of the calibration line (Fig. 11) were estimated using linear regression analysis in which the standard deviations of data points were introduced as weighting factors. The intercept shows high levels of Al contamination in the zero concentration phantom. Provided that

the MDL calculation is based on the uncertainty associated with the zero concentration phantom, higher purity phantoms are recommended for a more reliable investigation of the detection limit. MDL values were calculated with and without accounting for the goodness-of-fit. A statistical uncertainty of 16-18% was estimated for all MDL values reported in this work.

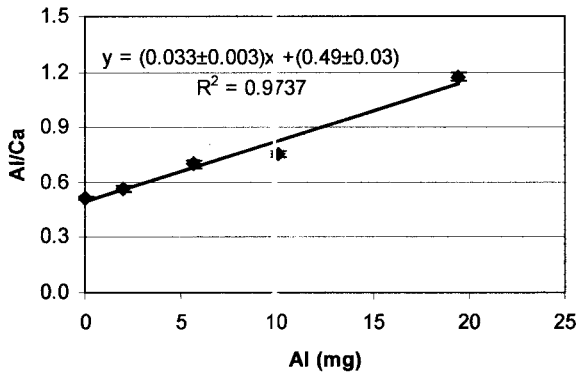

Fig. 11. Calibration line corresponding to resin phantoms set.

Table IV. Al/Ca ratios and associated uncertainties.

	Al/Ca	σ	$\sigma_{chi^2/v}$
ph#1	0.512	0.012	0.030*
ph#2	0.499	0.014	0.036*
ph#3	0.566	0.016	0.039*
ph#4	0.698	0.018	0.042*
ph#5	0.755	0.016	0.033*
ph#6	1.173	0.022	0.050*
	MDL (mg) =	**0.7**	**1.8 ***

*indicates reduced Chi-squared corrected values

Since the drawbacks that led to the high value of the reduced Chi-squared had been identified and can be corrected, these results can be improved upon. Ideally, when Chi-squared tends to 1, the corrected MDL should approach the uncorrected value. In this hypothesis, the uncorrected MDL value is significant for asserting the performance of the method. From the peak-to-total ratio in the Al standard, an improvement by a factor of ~1.7 was anticipated. Given the previously reported MDL value of 1.14mg (Pejovic-Milic, 2001), the new MDL value of 0.7mg validates this prediction.

It is perhaps more relevant to compare the spectral decomposition analysis MDL with the corresponding value, calculated by photopeak analysis, on the same data set. This was accomplished using the commercial software "Slide Write Plus 4.1", which allows the user to employ, among others, a Gaussian shape fitting function. A double Gaussian was therefore fitted over the partially overlapped photopeaks of chlorine and

Al, while for the background a simple straight line was used. This resulted in the following fitting equation:

$$y=(a_0/10)*\exp(-0.5*((x-a_1)/4)\text{^}2)+(a_2/11.25)*\exp(-0.5*((x-a_3)/4.5)\text{^}2+a_4-a_5*x$$

in which the six parameters are: a_0 – Cl peak area, a_1 – Cl peak centroid, a_2 – Al peak area, a_3 – Al peak centroid, a_4 – background intercept, a_5 – background slope. A prior 8-parameter fitting allowed the estimation of standard deviations for each peak; subsequently, in the equation above, the standard deviations were fixed to the calculated values ($\sigma_{Cl}=4, \sigma_{Al}=4.5$), reducing the number of variables and, implicitly, their uncertainties. For comparison, Fig. 12 reproduces the calibration slope obtained with data from the Slide Write fitting. As expected, the slope and intercept of this curve agree within uncertainties with those obtained using decomposition analysis, proving the consistency of the method. The MDL as calculated from the Slide Write fitting data was **1.7mg Al.** Accounting for 18% uncertainty in the MDL value, this value shows that an improvement with a factor of 2.3±0.6 may be achieved when data are analyzed by spectral decomposition analysis.

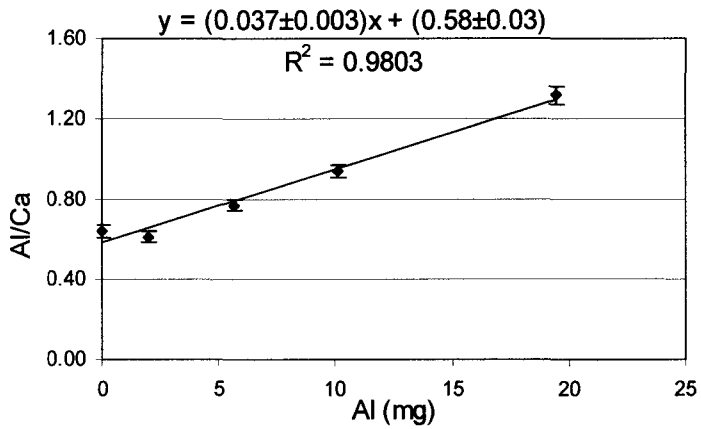

Fig. 12. Calibration line obtained for Slide Write data analysis.

This preliminary set of experiments has successfully shown the utility of spectral decomposition analysis and confirmed its improved sensitivity. Further investigation was

performed on a new set of higher purity phantoms, identical in size and shape to the standards. Furthermore, a time-dependent routine was added to the fitting algorithm, which was to be tested on spectra obtained with the new phantoms.

B. Aqueous solution phantoms were manufactured (chemical composition given in Section 2.2.3, Table III) in an attempt to improve phantom purity. Their chemical composition was validated against published spectra obtained from clinical trials on patients (Wyatt *et al.*, 1993).

An attempt was made to reproduce the irradiation parameters employed during earlier experiments (proton energy 2MeV, proton current 90μA or maximum achievable). It was however noticed that the performance of the lithium target averaged 15-17mRem/h on the Snoopy rem meter, compared with the previously observed range of 45-50mRem/h. This corresponded to a decrease of a factor of 2.4 in the Ca peak area, in a spectrum obtained following the same irradiation protocol, in the same resin phantom as the measurements in part **A.** Since the same proton energy was used, this was an indication that, for several possible reasons, the neutron yield was now lower.

The primary purpose of this new set of measurements was to test the fitting routine on spectra acquired in improved conditions (phantoms and standards of similar size and attenuation properties, and Iodine contribution to background eliminated by shielding the detectors). It was therefore decided to proceed with a higher energy proton beam (2.25MeV) and to adjust the current to a value that would result in ~50mRem/h on the Snoopy. A current of 80-85μA was thus measured on the target, and again, the current reading was considered accurate only to within 20%. Moreover, to account for the current fluctuations, a measurement of the integral charge was also recorded during the 180s phantom irradiation.

For observing changes in the target performance and for a more reliable monitoring of the neutron fluence, both the Snoopy and a long counter were employed. While Snoopy accounts also for the neutron energy distribution, the long counter is

characterized by a counting efficiency that is independent of the neutron energy, and consequently ideal for measurements of neutron flux.

Fig. 13 presents a model spectrum characteristic for the fitting results on water phantom spectra, together with the experimental data. Comparing the respective peak areas with those in Fig. 8, one can clearly see that the phantom activation was less successful in the new situation. This was assumed to be entirely due to the altered quality of the lithium target and to the different proton energy used. In this respect, the obtained MDL value (Table V) is not a significant indicator for the performance of the method and cannot be objectively compared to previous results.

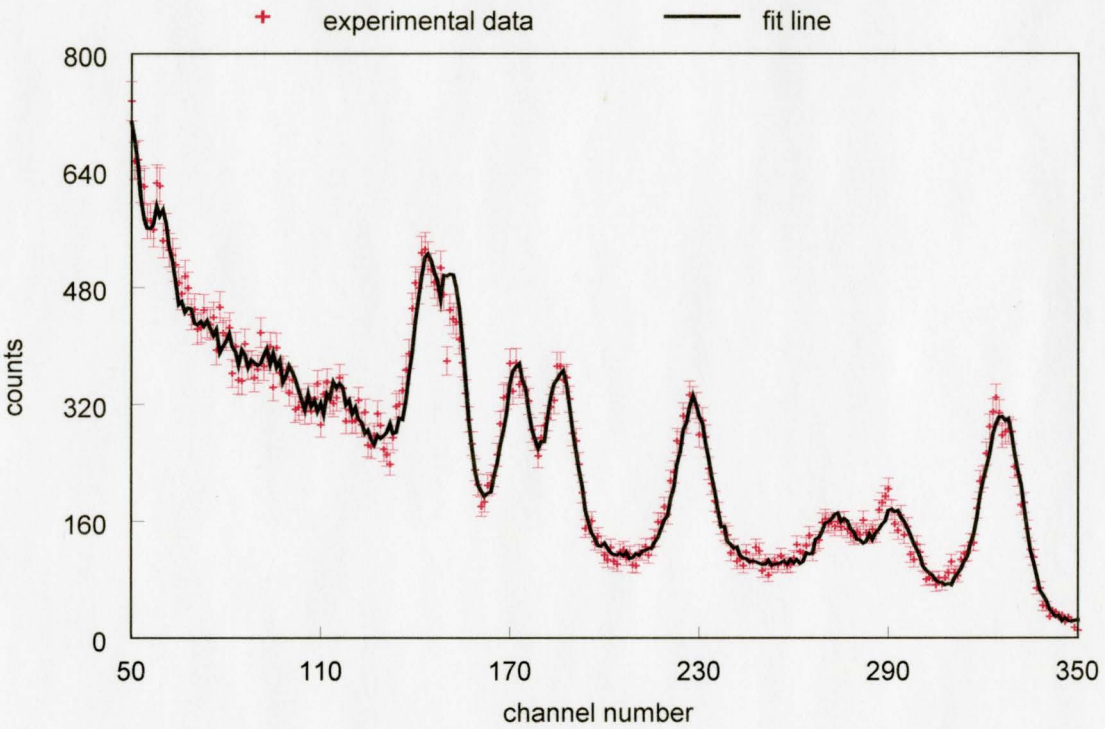

Fig. 13. Fitting of an aqueous solution phantom spectrum containing 10mg Al ($\chi^2/\nu = 1.6$).

Nevertheless, the reduced Chi-squared denotes a significantly improved goodness-of-fit. The experiment was therefore successful in showing that the activation of the NaI detectors was eliminated, or at least reduced to a magnitude that is no longer significant for spectral decomposition analysis. Moreover, the newly obtained intercept

(Fig. 14) is within uncertainty of zero, clearly showing the improvement achieved in phantom purity.

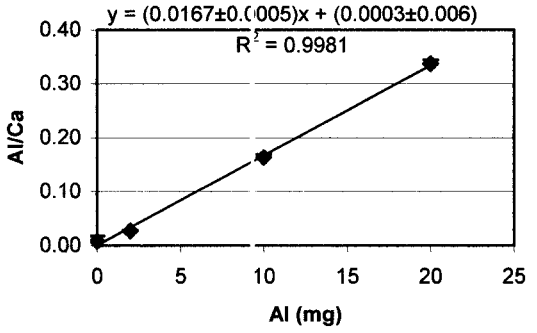

Fig. 14. Calibration line for aqueous solution phantoms set.

Table V. Al/Ca ratios and associated uncertainties.

	Al/Ca	σ	$\sigma_{chi^2/\sigma}$
ph#1	0.008	0.007	0.009
ph#2	0.027	0.0007	0.001
ph#4	0.164	0.005	0.006
ph#5	0.337	0.006	0.007
	MDL (mg) =	**0.9**	**1.1***

*indicates reduced Chi-squared corrected values

C. With the possibility of **replacing the lithium target** with a new one and the prospect of validating the method against a set of data acquired for what was considered optimal irradiation parameters, a new set of experiments was initiated. Along with the experimental developments, a new sub-routine was now included in the fitting program, which accounted for the known decay constants of each of the five elements contributing to the spectrum. For testing the time-dependant fitting routine, following the irradiation of the phantoms, a series of spectra were to be acquired instead of just one. The counting protocol was therefore adjusted to a phantom counting time of 150s and three subsequent spectra of the same phantom were collected.

With the newly prepared lithium target and after conditioning the accelerator, a Snoopy reading of 45mRem/h was achieved for 2MeV protons and a proton current of 180μA. The time-dependant fitting routine was therefore tested on the acquired spectra. An example of a spectrum and the obtained fitting is presented in Fig. 15. For all the fittings, the reduced Chi-squared values were in the 1.2 to 1.4 range. The Al/Ca contributions obtained from the fitting parameters and their standard deviations are presented in Table VI. Fig. 16 gives the calibration line used for MDL calculation.

Comparatively, the Slide Write fitting procedure yielded an MDL of **1.0±0.2mg Al** on the same set of data. An improvement by a factor of 1.4±0.4 was therefore obtained using spectral decomposition analysis.

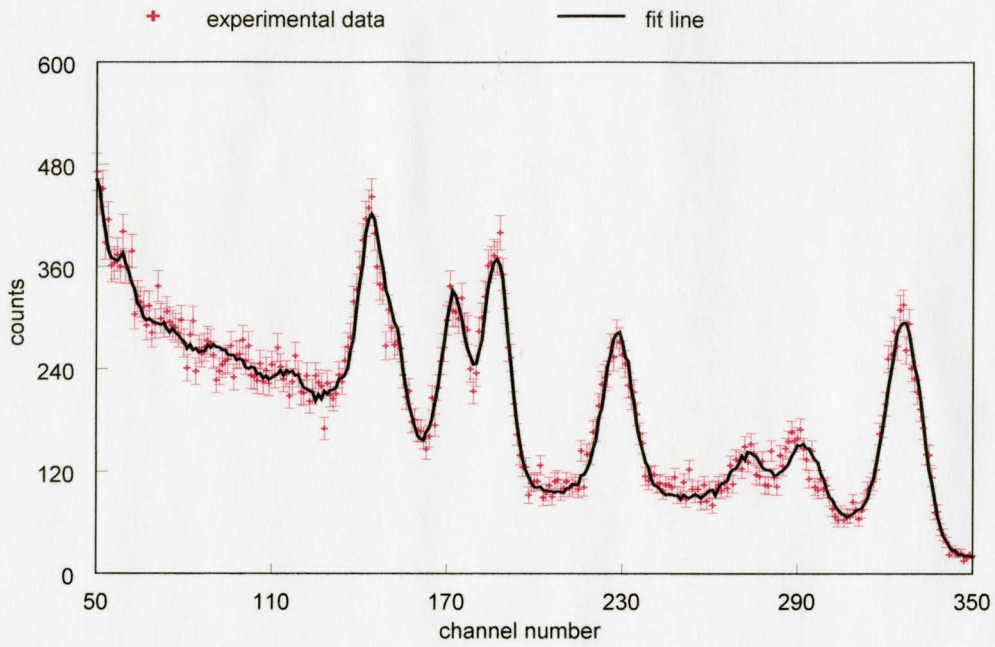

Fig. 15. Example of fitting using the time-dependent routine ($\chi^2/\nu = 1.26$).

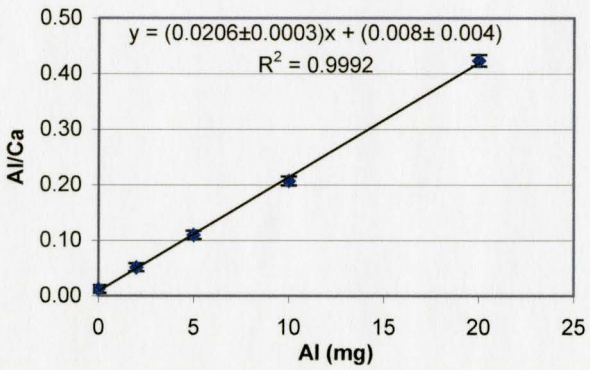

Fig. 16. Calibration line for time-dependent fitting routine data.

Table VI. Al/Ca ratios and associated uncertainties.

	Al/Ca	σ	$\varsigma_{chi^2/\nu}$
ph#1	0.012	0.006	0.007*
ph#2	0.051	0.006	0.007*
ph#3	0.110	0.007	0.008*
ph#4	0.207	0.007	0.008*
ph#5	0.42	0.009	0.01*
	MDL (mg) =	**0.6**	**0.7***

*indicates reduced Chi-squared corrected values

At this point, however, it was difficult to assess the particular contribution of the time-dependant fitting routine to the overall performance of the method. For this purpose, the data should be compared against a set of results obtained for spectra acquired in the same experimental conditions, namely with the new target, and analyzed with the regular fitting routine. Moreover, to investigate the reproducibility of the MDL, two more sets of irradiations were performed within a time interval of a week, for identical irradiation conditions: 2MeV proton energy and the maximum achievable proton current for which the Snoopy reading was below 45-50mRem/h.

Unexpectedly, the prior fitting performance could not be repeated: for both sets of data, the reduced Chi-squared was ~2.5. An analysis of the respective peak positions in standards versus phantoms demonstrated that the fitting routine is sensitive to detector gain shifts corresponding to less than one channel (~10keV). Also, it is worth mentioning that prior to any experiment, the gains were carefully matched using an acquisition software for which the precision in estimating peak centroids is also within one channel. Correlating these findings, it appears that the goodness-of-fit can always be situated in a range up to 2.5.

Regardless of this drawback, the calibration lines obtained showed good reproducibility of the experiments (Fig. 17); in addition, the MDL values were within the statistical errors (Table VII).

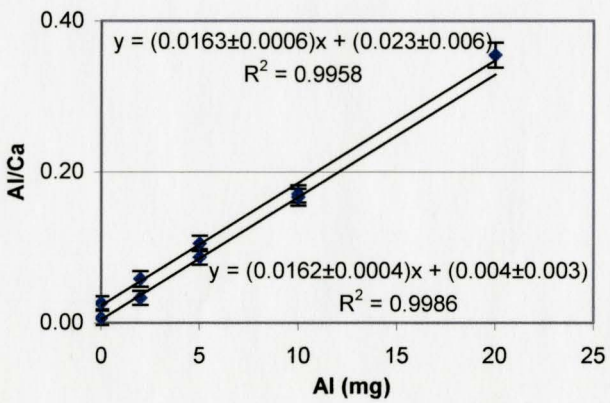

Fig. 17. Calibration lines corresponding to data from two different irradiation trials.

Table VII. MDL values (mg Al) obtained in two successive irradiation trials.

MDL	MDL*
0.7±0.1	1.1±0.2*
0.7±0.1	1.2±0.2*

*indicates reduced Chi-squared corrected values

Data in Table VII reveal that the MDL improvement achieved using time-dependent fitting routine is apparently not statistically significant. As reporting statistical uncertainty in the MDL is not a common practice in the specialized literature, this conclusion is debatable.

D. Dosimetry investigations do not fall within the scope of this study. However, the researched method cannot be affirmed as an improvement for the detection sensitivity unless the obtained MDL values had been achieved within the previously reported dose to a patient's hand of 48mSv (Pejovic-Milic, 2001).

A simple procedure utilizing the Snoopy detector served for the assessment of the neutron dose during the irradiation protocol. Earlier dosimetry and microdosimetry investigations (Arnold, 2000; Pejovic-Milic, 2001) showed that, at 10cm from the target, the Snoopy underestimates the neutron dose as measured by microdosimetry with an average factor of 1.3. This assessment could therefore be used to correlate Snoopy and microdosimetry measurements. Also, the microdosimetry measurements (Arnold, 2000) acknowledged that, inside the irradiation cavity, the gamma-ray dose represents up to 30% of the total dose. Consequently, once the neutron dose was evaluated, the total dose to hand could be extrapolated.

The investigation of the McMaster Accelerator as a neutron source has shown the non-uniformity of the neutron field. Microdosimetry measurements as a function of angle revealed that the dose drops to 50% for an angle of 30° off axis, to 10% for 60°, and to about 5% at 90° of its value along the beam axis (Arnold, 2000). To prevent the influence of the non-uniformity of the field upon the dose measurement, the Snoopy remmeter was positioned in front of the target, at a distance for which the solid angle that it subtended was equivalent to the solid angle corresponding to the investigated phantoms.

Assuming circular cross-sectional areas, equivalent radii were calculated for both the phantom and Snoopy's effective areas. As shown in the diagram in Fig. 18, the distance at which Snoopy should be positioned could thus be derived. The dose recorded with Snoopy at this position was then corrected for the distance by the inverse square

law. To prevent the occurrence of saturation in Snoopy, very low proton current (5μA) was used during the dosimetry measurements and the dose was then extrapolated for the current value used during phantom irradiations.

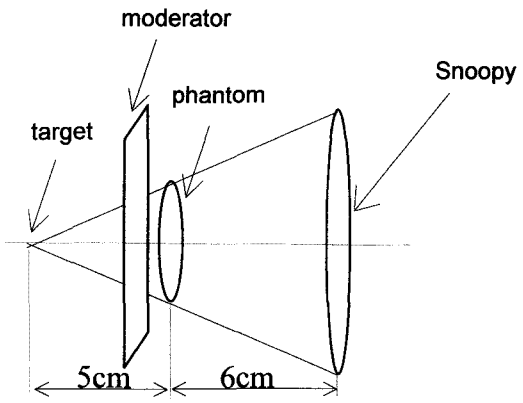

Fig. 18. Experimental setting for dosimetry measurements.

The linearity in the relationship between dose and the proton current was checked up to 15μA with satisfactory results (Fig. 19). However, for higher currents the steering and collimating of the beam and its centering onto the target becomes a more challenging task and the linearity between current and dose might be affected.

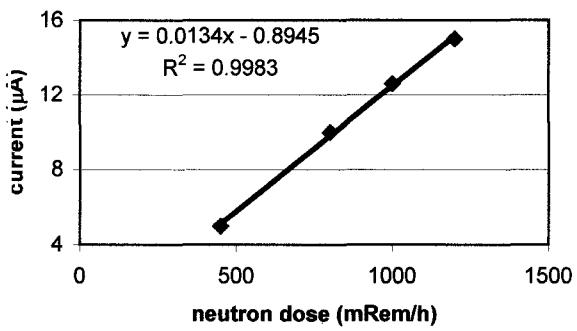

Fig. 19. Plot confirming the linearity of dose rate as measured by the Snoopy with the proton current on lithium target.

An average value of (2.00±0.01)mRem/h/μC was obtained for the dose rate during four irradiation trials at different proton currents (5, 10, 12.6, 15μA). The corresponding average integral charge accumulated over 180s of neutron irradiation using 2MeV protons was of $(11\pm1)x10^3$μC. This results in a neutron dose to a hand of 11mSv over the course of one irradiation. However, with the assumption that Snoopy underestimates the dose by a factor of 1.3, a value of 14.3mSv will be considered for the neutron dose. An additional contribution of 30% from the gamma-rays would lead to a total dose of **20.4mSv**. An uncertainty of 5% is usually associated with Snoopy remmeter measurements.

The previous microdosimetry measurements resulted, however, in a considerably higher local dose (48mSv)(Pejovic-Milic, 2001). The dose rates obtained by microdosimetry when using the quality factors reported by ICRP 26 were 0.12mSv/s/μA, in the center of the irradiation cavity, and 0.03mSv/s/μA, at 7cm off the central axis (Arnold, 2000). One can see that, 7cm away from the beam axis, the dose drops to 25% (total length off-axis of the phantom is 10cm). Knowing that Snoopy was also calibrated using ICRP26 quality factors, the dose rate of 0.02mSv/s/μA obtained in the current study seems somewhat reasonable. It is worth emphasizing that the practice of normalizing the doses on the beam current introduces a major uncertainty factor. For example, the current range for which the dose rate of 45-50mRem/h on Snoopy could be reproduced on the course of this study, at different time intervals, was 55-180μA.

It appears thus that a major factor leading to discrepancies in the dose estimations may be the normalization to a beam current with large uncertainties. Nevertheless, recent technical improvements to current reading allowed a more reliable estimation of the proton current: during the dosimetry measurements, the current on target was 92% of the current indicated on the third Faraday cup. We therefore conclude that the new MDL of **(0.7±0.1)mg Al** was achieved for a total dose to a hand of **(20±1)mSv**.

Chapter 4. Conclusions and future directions

Of the two approaches considered in this study, spectral decomposition analysis of data contributed significantly to the performance of McMaster *in vivo* Al detection system. Using spectral decomposition analysis within NAA, an estimated improvement factor of 1.7 could be achieved in the MDL, compared to when data analysis is based on the traditional Marquardt method, which accounts only for the information in the Al photopeak. Phantom measurements proved indeed that the new MDL (0.7±0.1mg Al) is lower by a factor of 1.60±0.04 than the MDL reported in a previous study (1.14mg Al)(Pejovic-Milic, 2001).

A time-dependent fitting routine was developed and tested on a series of three spectra acquired each over 150s. At this stage, the improvement in the sensitivity was not statistically significant (MDL=(0.60±0.01)mg Al). However, the additional information exploited by the method, namely the decaying constants of the different isotopes in a hand, should definitely contribute to refining the MDL. In exploring the time-dependent procedure, one should further investigate the optimal number of spectra and their acquisition times as allowed by the half-life of Al that would minimize the MDL.

A limiting factor in the performance of spectral decomposition analysis was the goodness-of-fit parameter Chi-squared. Values above 2 for this parameter were obtained throughout this study. The fact that Chi-squared departs from 1 is attributable to a slight misalignment of the standards with the phantom spectra, as a result of gain shifts on the NaI detectors. Two solutions could be envisioned for this problem: the replacement of the resistors in the photomultiplier tubes with Zener diodes, or, simply, the inclusion of a sub-routine in the fitting algorithm to compensate for the respective shifts in the spectra.

In addition, a data filtering procedure can be examined within spectral decomposition analysis. By convolution with the standard spectra, a symmetrical zero-area filter would remove any background contribution to the spectrum (Robertson *et al.*,

1972). An optimal filter applied to both the standard and phantom spectra would therefore assure an increased specificity in the assessment of the number of counts. While this would not guarantee any gain to the sensitivity of the method, it should serve for evaluating the accuracy with which *in vivo* levels of Al can be predicted.

The routine monitoring of the radiation levels during phantom irradiation using a Snoopy remmeter insured that the reported MDL was not achieved to the detriment of the dose to the patient. During all experiments, the proton current was set to a value for which the dose rate as monitored by the Snoopy was in the 45-50mRem/h range. This dose rate range, measured at a standard position with respect to the target, was previously reported to correspond to a dose to hand below 50mSv (Pejovic-Milic, 2001). In addition to routine monitoring, the local dose delivered during 180s irradiation was estimated based on the following approach. A correlation factor of 1.3 was reported between the microdosimetry experiments and the neutron dose as measured by Snoopy (Arnold, 2000). Therefore, knowing that the neutron dose measured by the Snoopy represents 70% of the total dose (30% being the gamma dose contribution (Arnold, 2000)), the total dose to the hand could be extrapolated. The total dose to the hand as measured in this study averaged (20±1)mSv. The fact that the dose reported in this study is considerably lower then the 48mSv dose estimated in the prior study (Pejovic-Milic, 2001) can be explained by a series of factors. Firstly, since the doses are normalized onto the target current, the large uncertainties in target current reading, despite repeated attempts at improving electron suppression, are unavoidably reflected in the estimation of doses. In addition, a factor of up to 1.5 in the microdosimetry doses can be gained when using ICRP 60 neutron quality factors, rather than ICRP 26.

A second approach of this study, the electronic elimination of coincidences from the gamma spectrum of an activated phantom, while not significant for the results reported here, was proved as a promising valuable tool for a system with increased detection efficiency. Indeed, preliminary results on a newly developed detection system showed that the detection of coincidences in a gamma spectrum could be increased by a factor of 10 compared to the performance of the system used for the current application.

A more thorough investigation of the advantages of removing the coincidences from the spectra is projected.

As the sensitivity of the investigated detection method should be reported as mg of Al per dose to the patient, is probably important to emphasize that an irradiation cavity (moderator/shielding assembly) designed based on Monte Carlo neutron transport simulations (Pejovic-Milic, 2001) is currently under development. The addition of this irradiation assembly to the procedure will considerably diminish the dose received by the patient. Moreover, a new portable accelerator, capable of achieving proton current in the mA range will soon be commissioned within the NAA facility at McMaster. The possibility of increasing the proton current (increased thermal neutron fluence rate), and correspondingly adjust the irradiation parameters is expected to contribute to the improvement of the MDL, with the least effect on the delivered dose. In the limit of short irradiations, an MDL of 0.5mg Al can therefore be predicted.

This study reports a new MDL value of **0.7mg Al,** achieved for a total dose to a hand of **(20±1)mSv**. While the reported MDL value is still above the normal levels of Al in the hand of a patient, the mentioned improvements and additions to the method would certainly further increase its sensitivity per dose to the patient. Moreover, clinical studies would eventually contribute to establishing an updated baseline of Al levels in healthy subjects.

Bibliography

Alfrey, A.C., *Aluminum intoxication*, N. Engl. J. Med. 310, 1113-1115, 1984.

Alfrey, A.C., *Aluminum metabolism in uremia,* Neurotoxicology 1, 43-53, 1980.

Alfrey, A.C., LeGendre, G.R., Kaehny, W.D., *The dialysis encephalopathy syndrome. Possible aluminum intoxication*, N. Engl. J. Med. 294, 184-188, 1976.

Anthony, J., Fadl, S., Mason, C., Davidson, A., Berry, J., *Absorption, deposition and distribution of dietary aluminum in immature rats: Effects of dietary vitamin D3 and food-borne chelating agent*, J. Environ. Sci. Health B21, 191-205, 1986.

Arnold, M., *Development of an accelerator based system for in vivo neutron activation analysis measurements of manganese in humans*, Ph.D. thesis, McMaster University, 2000.

Aslam, Prestwich, W.V., McNeill, F.E., Waker, A.J., *Investigating the TEPC radiation quality factor response for low energy accelerator based clinical applications*, Radiat. Prot. Dosimetry 103(4), 311-322, 2003a.

Aslam, Prestwich, W.V., McNeill, F.E., Lithium target performance evaluation for low-energy accelerator-based in vivo measurements using gamma spectroscopy, Appl. Rad. Isot. 58, 321-331, 2003b.

Aslam, Prestwich, W.V., McNeill, F.E., Waker, A.J., *Spectrometry and dosimetry for low energy accelerator based in-vivo measurements*, Annual Report McMaster Accelerator Laboratory, McMaster University, Hamilton, ON, Canada, 2001.

ATSDR (Agency for Toxicological Substances and Disease Registry): *Toxicological profile for aluminum*, U.S. Department of Health and Human Services, Public Health Service (visit http://www.atsdr.cdc.gov/toxprofiles/tp22.html), 1999.

Bakir, A.A., Hryhorczuk, D.O., Berman, E., Dunea, G., *Acute fatal hyperaluminemic encephalopathy in undialyzed and recently dialyzed uremic patients*, ASAIO Trans. 32, 171-176, 1986.

Berand, K., van der Voet, G., Boer, W.H., *Acute aluminum encephalopathy in a dialysis center caused by cement mortal water distribution pipe*, Kidney Int. 59, 746-753, 2001.

Bevington, P.R., Robinson, D.K., *Data Reduction and Error Analysis for the Physical Sciences*, 2nd ed., McGraw-Hill Inc., 1992.

Birks, J.B., *The theory and practice of Scintillation Counting*, Pergamon Press, Oxford, 1964.

Bishop, N.J., Morley R., Day, J.P., Lucas A., *Aluminum neurotoxicity in preterm infants receiving intravenous feeding solutions*, New England Journal of Medicine 336, 1557-1561, 1997.

California Environmental Protection Agency, Office of Environmental Health Hazard Assessment, *Public Health Goal for Aluminum In Drinking Water* (visit http://www.oehha.ca.gov/water/phg/pdf/Aluminumf.pdf), April 2001.

Cannata-Andia, J.B. and Fernandez-Martin, J.L., *The clinical impact of aluminum overload in renal failure*, Nephrol. Dial. Transplant 17, Suppl. 2, 9-12, 2002.

Chan, J.C.M., Jacob, M., Brown, S., Savory, J., Wills, M.R., *Aluminum metabolism in rats; Effects of vitamin D dihydrocortisol, 1,25-dihydroxyvitamin D and phosphate binders*, Nephron. 48, 61-64, 1988.

Cohn, S.H., *The present state of in vivo neutron activation analysis in clinical diagnosis and therapy,* Energy Rev. 18(3), 599-660, 1980.

Connor, M.O., Garrett, P., Dockery, M., Donohoe, J.F., Doyle, G.D., Carmody, M., Dervan, P.A., *Aluminum-related bone disease. Correlation between symptoms, osteoid volume, and aluminum staining*, Am. J. Clin. Pathol. 86(2), 168-174, 1986.

D'Haase, P.C., Coutteye, M.M., Goodman, W.G., *The use of desferroxamine test to diagnose and differentiate between patients with aluminum related bone disease increased risk for aluminum toxicity or aluminum overload*, Nephrol. Dial. Transplant. 10, 1874-1888, 1995.

Deng, Z., Coudray, C., Gouzoux, L., Mazur, A. Royssiguier, Y., Pepin, D., *Effects of acute and chronic coingestion of $AlCl_3$ with citrate or polyphenolic acids on tissue retention and distribution of aluminum in rats*, Biol. Trace Elem. Res. 76, 245-256, 2000.

Di Paolo, N., Masti, A., Comparini, I.B., Garosi, G., Di Paolo, M., *Uremia, dialysis and aluminum*, Int. J. Artif. Organs 20, 547-552, 1997.

Ellis, H.A., Mawhinney, W.H., *Aluminum Induced osteomalacia*, J. Clin. Path. 35, 792-793, 1982.

Ellis, K. J., Kelleher, S. P., *In vivo bone aluminium measurements in patients with renal disease. In Vivo Body Composition Studies* ed. Ellis, K. J., Yasumura, S. and Morgan, W. D., London, 1987.

Ellis, K. J., Kelleher, S., Raciti, A., Savory, J., Wills, M., *In vivo monitoring of skeletal aluminium burden in patients with renal failure*, J. Radioanal. Nucl. Chem. 124, 85-95, 1988.

Faugere, M.C., Malluche, H.H., *Stainable aluminum, and not aluminum content, reflects bone histology in dialyzed patients,* Kidney Int. 30(5), 717-722, 1986.

Fernandez-Martin, J.L., Canteros, A., Alles, A., Massari P., Cannata-Andia, J., *Aluminum exposure in chronic renal failure in iberoamerica at the end of the 1990s: Overview and perspectives*, Am. J. Med. Sci. 320, 96-99, 2000.

Flarend, R., Bin, T., Elmore, D., Hem, S.L., *A preliminary study of the dermal absorption of aluminium from antiperspirants using aluminium-26*, Food Chem. Toxicol. 39, 163-168, 2001.

Flaten, T.P., *Aluminium as a risk factor in Alzheimer's disease, with emphasis on drinking water*, Brain Res. Bull. 55, 187-196, 2001.

Green, S.R., Chettle, D.R., *A feasibility study of the in vivo measurement of aluminium in peripheral bone*, Phys. Med. Biol. 31, 2387-2396, 1992.

Greger, J.L. Goetz, W., Sullivan, D., *Aluminum levels in food cooked and stored in aluminum pans, trays and foil*, J. Food Prot. 48, 772-777, 1985.

Hjortsberg, U., *Association between exposure to potassium aluminum tetrafluoride and bronchial hyperractivity and asthma*, Scand. J. Work Environ. Health. 25(5), 457, 1999.

ICRP 23, Report of the task group on Reference Man, Pergamon Press, Oxford, 1975.

IDSP (Industrial Disease Standards Panel, Toronto, Ontario), *Interim Report to the Workers' Compensation Board on Aluminum, Report of Findings No. 9* (visit http://www.canoshweb.org/odp/html/MAY1992.htm), 1992.

Jansson, E.T., *Aluminum exposure and Alzheimer's disease*, J. Alzheimer's Dis. 3(6), 541-549, 2001.

Jarava, C., Armas, J.R., Palma, A., *Aluminum and uremic bone disease. Diagnostic utility of serum aluminum and the deferoxamine (DFO) test*, Nefrologia 21(2), 174-181, 2001.

Jeffery, E.H., Abreo, K., Burgess, E., Cannata, J.B., Greger, J.L., and Zaman, K., *Aluminum effects on bone formation and remodeling, hematopoiesis and renal function*, J. Toxicol. Environ. Health 48, 649-665, 1996.

Kausz AT, Antonsen JE, Hercz G, Pei Y, Weiss NS, Emerson S, Sherrard DJ., *Screening plasma aluminum levels in relation to aluminum bone disease among asymptomatic dialysis patients*, Am. J. Kidney Dis. 34(4), 688-693, 1999.

Knoll, G.F., *Radiation detection and measurement*, 3rd ed., John Wiley and Sons, New York, 2000.

Lin, J.L., Yang, Y.J., Yang, S.S., Leu, M.L., *Aluminum utensils contribute to aluminum accumulation in patients with renal disease*, Am. J. Kidney Dis. 30, 653-658, 1997.

Lione, A., *The prophylactic reduction of aluminum intake*, Food Chem. Toxicol. 21, 103-109, 1983.

Maitani, T., Kubota, H., Hori, N., Yoshihira, K., Takeda, M., *Distribution and urinary excretion of aluminium injected with several organic acids into mice: relationship with chemical state in serum studied by the HPLC-ICP method*, J. Appl. Toxicol. 14(4), 257-61, 1994.

Makjanic, J., McDonald, B., Li-Hsian, C.P., Watt, F., *Absence of aluminium in neurofibrillary tangles in Alzheimer's disease*, Neurosci. Lett. 240(3), 123-126, 1998.

Malluche, H.H., *Aluminium and bone disease in chronic renal failure*, Nephrol. Dial. Transplant 17, Suppl. 2, 21-4, 2002.

Maloney, N.A., Ozt, S.M., Alfrey, A.C., *Histological quantitation of aluminum in iliac bone from patients with renal failure*, J. Lab. Clin. Med. 99, 206-216, 1982.

Matsumoto, H., *Cell biology of aluminum toxicity and tolerance in higher plants*, Int. Rev. Cytol. 200, 1-46, 2000.

Morgan, W.D., McNeil, E.A., Wyatt, R.M., Ryde, S.I.S., Evans, C.J., Dutton, J., Sivyer, A., Williams, A.J., *Development of a technique to measure bone aluminium in vivo using a Cf-252 source. In Vivo Body Composition Studies: Recent Advances* ed. Yasumun, S., Harrison, J.G., McNeil, K.J., Woodhead, A.D., Dilmanian F.A., New York Plenum, 1990.

Nayak, P., *Aluminum: Impacts and Disease,* Environ. Res. Sect. A 89, 101-115, 2002.

O'Meara, J., *Measuring lead, mercury and uranium by in-vivo X-ray fluorescence,* Ph.D. thesis, McMaster University, 1999.

Ortec, Application Note 59, Gedcke, D.A., *How counting statistics controls detection limits and peak precision* (visit http://www.ortec-online.com/application-notes/an59.pdf), 2001.

Ott, S.M., Maloney, N.A., Klein, G.L., *Aluminum is associated with low bone formation in patients receiving chronic parenteral nutrition*, Ann. Intern. Med. 98, 910-914, 1983.

Owen, L.M., Crews, H.M., Bishop, N.J., Massey, R.C., *Aluminium uptake from some foods by guinea pigs and the characterization of aluminium in in vivo intestinal digesta by SEC-ICP-MS*, Food Chem. Toxicol. 32(8), 697-705, 1994.

Palerme, S., *Pilot studies for in vivo bone aluminum measurements*, M.Sc. Thesis, McMaster University, 1993.

Pejovic-Milic, A., *An accelerator based in vivo measurement of aluminum in human bone by neutron activation analysis*, M.Sc. Thesis, McMaster University, 1998.

Pejovic-Milic, A., *In Vivo measurements of aluminum and strontium in human bone*, Ph.D. Thesis, McMaster University, 2001.

Pengloan, J., Dantal, J., Rossazza, C., Abazza, M., Nivet, H., *Ocular toxicity after a single intravenous dose of desferrioxamine in two hemodialyzed patients*, Nephron. 46, 211-212, 1987.

Riihimäki, V., Hänninen, H., Akila, R., Kovala, T., Kuosma, E., Paakkulainen, H., Valkonen, S., Engström, B., *Body burden of aluminum in relation to central nervous system function among metal inert-gas welders*, Scand. J. Work Environ. Health 26(2), 118-130, 2000.

Robertson, A., Prestwich, W.V., Kennett, T.J., *An automatic peak-extraction technique*, Nucl.Instr. and Methods 100, 317-324, 1972.

Röllin, H.B., Theodorou, P., Kilroe-Smith, T.A., *Deposition of aluminium in tissues of rabbits exposed to inhalation of low concentrations of Al_2O_3 dust.* British J. Ind. Med. 48, 389-391, 1991.

Rondeau, V., *A review of epidemiologic studies on aluminum and silica in relation to Alzheimer's disease and associated disorders*, Rev. Environ Health. 17(2), 107-21, 2002.

Sebes, J, *Aluminum induced bone and joint disease overview and current perspective*, Osteologiai Kozlemenyek 1, 17-22, 2003.

Van Landeghem, G.F., D'Haese, P.C., Lamberts, L.V., De Boer, M.E., *Quantitative HPLC/ETAAS hybrid method with an on-line metal scavenger for studying the protein binding and speciation of aluminum and iron,* Anal. Chem. 66(2), 216-222, 1994.

Venturini-Soriano, M., Berthon, G., *Aluminum speciation studies in biological fluids. Part 7. A quantitative investigation of aluminum(III)-malate complex equilibria and their potential implications for aluminum metabolism and toxicity*, J. Inorg. Biochem. 85, 143-154, 2001.

Wilhelm, M., Hohr, D., Abel, J., Ohnesorge, F.K., *Renal aluminum excretion*, Biol. Trace Elem. Res. 21, 241-245, 1989.

Wilhelm, M., Jäger, D.E., Ohnesorge, F.K., *Aluminum toxicokinetics*, Pharmacol. Toxicol. 66, 4-9, 1990.

Wyatt, R.P., Ryde, S.J.S., Morgan, W.D., McNeil, E.A., Hainsworth, I.R., Williams, A.J., *The development of a technique to measure bone aluminum content using neutron activation analysis*, Physiol. Meas. 14, 327-335, 1993.

Yokel, R.A. and McNamara, P.J., *Aluminum Toxicokinetics: An updated MiniReview*, Pharmacol.&Toxicol. 88, 159-167, 2001.

Yokel, R.A., McNamara, P.J., *Aluminum bioavailability and disposition in adult and immature rabbits*, Toxicol. Appl. Pharmacol. 77, 344-352, 1985.

Ysart, G., Miller, P., Croasdale, M., Crews, H., Robb, P., Baxter, M., de L'Argy, C., Harrison, N., *1997 UK Total Diet Study; Dietary exposures to aluminium, arsenic, cadmium, chromium, copper, lead, mercury, nickel, selenium, tin and zinc*, Food Addit. Contam. 17, 775-786, 2000.

Zafar, T.A., Weaver, C.M., Martin, B.R., Flarend, R., Elmore, D., *Aluminum (^{26}Al) metabolism in rats*, Proc. Soc. Exp. Biol. Med. 216(1), 81-85, 1997.